International Journal for Numerical Methods in Engineering

WILEY

RESEARCH ARTICLE OPEN ACCESS

Control Variates Method to Estimate Stochastic Buckling Loads

Marc Fina[1] | Marcos A. Valdebenito[2] | Werner Wagner[1] | Matteo Broggi[3] | Steffen Freitag[1] | Matthias G. R. Faes[2,4] | Michael Beer[3,4,5]

[1]Institute for Structural Analysis, Karlsruhe Institute of Technology, Karlsruhe, Germany | [2]Chair for Reliability Engineering, TU Dortmund University, Dortmund, Germany | [3]Institute for Risk and Reliability, Leibniz University Hannover, Hannover, Germany | [4]International Joint Research Center for Resilient Infrastructure & International Joint Research Center for Engineering Reliability and Stochastic Mechanics, Tongji University, Shanghai, PR China | [5]Department of Civil and Environmental Engineering, University of Liverpool, Liverpool, UK

Correspondence: Marc Fina (marc.fina@kit.edu)

Received: 23 April 2025 | **Revised:** 23 April 2025 | **Accepted:** 4 June 2025

Funding: Deutsche Forschungsgemeinschaft (DFG, German Research Foundation) in the framework of project 511267658.

Keywords: buckling analysis | control variates | monte carlo simulation | random imperfections | second-order statistics

ABSTRACT

Buckling is the most significant failure mode for thin-walled structures. In particular, geometric imperfections have a major influence on the buckling behavior. These spatially correlated imperfections are inherently random and can be modeled using random fields. Therefore, computationally expensive probabilistic buckling analyses have to be performed. For some structures, a linear pre-buckling behavior can be observed. In this case, the stability point can be calculated with a linear buckling analysis, which is widely used in engineering practice. However, the results of linear buckling analyses strongly differ from the correct buckling load in the case of a non-linear pre-buckling behavior. Then, a non-linear buckling analysis is required, which is computationally expensive for probabilistic safety assessments based on Monte Carlo simulations. This paper aims to estimate the second-order statistics of buckling loads for thin-walled structures exhibiting strongly non-linear pre-buckling behavior. The estimation leverages existing correlations between the outcomes of linear and non-linear buckling analyses. The proposed approach utilizes the framework of Control Variates, wherein the more expensive analysis (non-linear buckling analysis) is run a few times only, while the cheaper linear buckling analysis is run a considerable number of times. The proposed method is demonstrated on a variety of structures, including a folded plate with multiple types of stability points, a composite shell panel, and a cylinder with random geometric imperfections. In these numerical examples, stochastic buckling analysis using Control Variates is approximately 1.5 to 2.6 times faster than classical Monte Carlo simulation.

1 | Introduction

One of the dominant failure modes of thin-walled structures is buckling. Geometric and material imperfections, such as deviations in shape and thickness, residual stresses, variations in boundary conditions, and material properties, have a substantial influence on the buckling behavior. Even small variations in geometric imperfections significantly influence the load-bearing capacity. The exact shape of imperfections is frequently unknown, or in other words, uncertain. Deterministic and semi-probabilistic design concepts are based on very conservative design factors, also known as knockdown factors (KDFs).

The development of reliable and more economical KDFs remains a focus of numerous ongoing research projects, as illustrated, for example, in Reference [1].

In a probabilistic approach, the aleatory uncertainties of spatially varying imperfections are modeled as random fields, see, for example, in References [2–4]. In this paper, random imperfections are applied to the finite element (FE) model, and Monte Carlo simulations (MCS) are conducted to determine the second-order statistics of random buckling loads. However, to quantify the uncertain shape of the geometrical imperfections, only a few measurements are available. The definition of deterministic random field parameters under these limited data would imply precise probabilistic knowledge on the stochastic distribution and its spatial correlation. Therefore, in References [5–7], the concept of polymorphic (mixed/hybrid) uncertainty models [8], also known as imprecise probabilities [9, 10], is introduced to consider epistemic uncertainties of shell imperfections by means of intervals or fuzzy numbers. An extension to quantify the uncertainties in boundary conditions, material properties, and thickness imperfections is provided in Reference [11]. This paper initially explores the feasibility of using the Control Variates method for stochastic buckling analyses, with an emphasis on the spatial correlation of random imperfections. A potential extension of this work could involve applying the method to address polymorphic uncertainty, such as random fields with interval or fuzzy correlation lengths.

A numerical treatment of aleatory and epistemic uncertainties requires a multi-loop algorithm consisting of the fundamental solution (e.g., FE buckling analysis), the MCS loop, and the fuzzy or interval analysis. This can be highly computationally expensive, and the effort increases rapidly for buckling design optimization, as illustrated in Reference [12]. Additionally, when geometric imperfections are applied to an FE model, the geometrical deviation at each node is a single input variable. This leads to a high-dimensional input space of uncertain variables. Therefore, appropriate surrogate models can be used to replace the time-consuming FE analysis. For instance, an approach for efficiently analyzing the imperfection sensitivity using reduced order models is presented in References [13, 14]. Furthermore, neural network surrogate models to approximate FE buckling analysis are shown in References [15, 16]. Based on a first surrogate model for the fundamental solution, a further surrogate model can be constructed to replace the MCS, see, for example, [17]. An approach for bounding imprecise failure probabilities of linear structural systems is introduced in Reference [18]. However, this approach is not applicable to non-linear buckling problems, as it relies on the assumption of a linear mapping between input and output quantities within the used operator norm theory.

This paper aims to estimate the second-order statistics (mean and standard deviation) of the buckling loads of thin-walled shell structures, with imperfections characterized by probabilistic models. The proposed approach is based on the concept of Control Variates [19], which has been studied in various engineering applications, such as [20–22]. The main contribution of this work is to introduce Control Variates for probabilistic buckling analysis, where geometric imperfections are modeled as random fields. The idea is to leverage the existing correlations between the solutions of linear and non-linear buckling analyses.

In case of non-linear pre-buckling behavior, a non-linear buckling analysis provides an accurate prediction of the buckling load, and a linear buckling analysis leads to imprecise results. It should be noted that for some structures with a linear pre-buckling behavior, the linear buckling analysis can still yield an incorrect prediction due to buckling mode interaction. However, in case of multiple buckling loads nearly at the same level, for example, for an axially loaded cylinder, the "exact" buckling load can be calculated, and the shape of the associated buckling mode is not relevant. Furthermore, the non-linear buckling analysis requires a geometrically non-linear path-following analysis involving an iterative procedure. Therefore, the linear buckling approach is typically less computationally expensive than the non-linear buckling analysis. Second-order statistics are determined by sampling, involving a limited number of non-linear analyses and a relatively large number of linear buckling analyses. Thus, the presented Control Variates approach reduces overall computational costs, as the more expensive non-linear buckling analysis is performed only a few times, while the less costly linear buckling analysis is executed more frequently. Furthermore, by exploiting the correlation between linear and non-linear analyses, it is still possible to estimate the statistics of the accurate buckling load, even when the linear buckling analysis is applied to cases with strong non-linear pre-buckling behavior.

In this paper, the Control Variates approach is demonstrated for stochastic buckling analysis of a composite cylindrical shell panel. Random geometric imperfections are modeled as random fields using the Karhunen-Loève Expansion (KLE). The shape of the random imperfection can be controlled by the correlation length. Thus, second-order statistics of the buckling loads are analyzed for various correlation lengths using Monte Carlo simulations (MCS). To illustrate the applicability of Control Variates, the correlation between linear and non-linear buckling analysis is investigated. The effectiveness of Control Variates in estimating the second-order statistics of buckling loads is demonstrated on various thin-walled structures, including a folded plate with different types of stability points, a composite shell panel, and a cylinder subjected to random geometric imperfections with varying correlation lengths.

The paper's innovative contributions and key features can be summarized as follows:

- Introduction of Control Variates with splitting technique for stochastic buckling analyses
- Efficient estimation of the second-order statistics of buckling loads
- Leveraging correlations between linear and non-linear buckling analyses
- Random field modeling with Control Variates
- Study on the effectiveness of Control Variates for various correlated random geometric imperfections

- Stochastic buckling analysis using Control Variates is approximately 1.5 to 2.6 times faster than classical Monte Carlo simulation

In Sections 2 and 3, the fundamentals of numerical buckling analysis and the estimation of second-order statistics using Monte Carlo simulations are presented. Following this, the Control Variates approach for buckling is introduced in Section 4. Section 5 illustrates the concept on three different examples: a folded plate, a composite shell panel, and a composite cylinder. Finally, Section 6 provides conclusions and outlines potential directions for future research.

2 | Basics of Linear and Non-Linear Buckling Analysis

Various strategies are available for identifying a stability point, as discussed, for example, in References [23, 24]. For a specific load level $\lambda \boldsymbol{P}_0$ with a load factor λ and a basic external load $\boldsymbol{P}_0$, a non-linear eigenvalue problem can be constructed

$$[\boldsymbol{K}_{\text{lin}} + \Lambda \boldsymbol{K}_{\text{nlin}}]\, \boldsymbol{\varphi} = \boldsymbol{0} \tag{1}$$

where it is assumed that

$$\boldsymbol{P}_{\text{cr}} \sim \Lambda \boldsymbol{K}_{\text{nlin}} \tag{2}$$

In Equation (1), Λ can be interpreted as a load increasing factor, and $\boldsymbol{\varphi}$ is the associated eigenvector. The tangent stiffness matrix $\boldsymbol{K}_T$ is divided in linear $\boldsymbol{K}_{\text{lin}}$ and non-linear parts $\boldsymbol{K}_{\text{nlin}}$. Generally, the tangent stiffness matrix depends on the displacement $\boldsymbol{u}$ and stress state $\boldsymbol{\sigma}(\boldsymbol{u})$, respectively. If the variational formulation allows to separate $\boldsymbol{K}_{\text{nlin}}$, the initial displacement matrix $\boldsymbol{K}_U$ and the geometrical matrix $\boldsymbol{K}_G$ can be introduced

$$\boldsymbol{K}_T = \boldsymbol{K}_{\text{lin}} + \boldsymbol{K}_{\text{nlin}} = \boldsymbol{K}_{\text{lin}} + \boldsymbol{K}_U(\boldsymbol{u}) + \boldsymbol{K}_G(\boldsymbol{\sigma}(\boldsymbol{u})) \tag{3}$$

A solution for $\Lambda = 1$ in Equation (1) yields the classical form of an eigenvalue problem for the tangent stiffness matrix

$$(\boldsymbol{K}_{\text{lin}} + \Lambda \boldsymbol{K}_{\text{nlin}})\boldsymbol{\varphi} = \boldsymbol{0} \Leftrightarrow \boldsymbol{K}_T \boldsymbol{\varphi} = \boldsymbol{0} \Leftrightarrow (\boldsymbol{K}_T - \omega \boldsymbol{1})\boldsymbol{\varphi} = \boldsymbol{0} \tag{4}$$

wherein a stability point is indicated for $\omega = 0$. In the non-linear case, the eigenvalue Λ is an indicator of the type of stability

$$\begin{aligned} \Lambda > 1 &\rightarrow \text{stable} \\ \Lambda = 1 &\rightarrow \text{indifferent (stability point)} \\ \Lambda < 1 &\rightarrow \text{unstable} \end{aligned} \tag{5}$$

Furthermore, the non-linear critical load vector can be computed by

$$\boldsymbol{P}_{\text{cr}} = \boldsymbol{P}_{\text{cr,nlin}} = \Lambda(\lambda \boldsymbol{P}_0) \quad \text{with} \quad \Lambda = 1 \tag{6}$$

In addition, the type of stability point can be determined by the following criterion, see, for example, [25, 26],

$$\boldsymbol{\varphi}^T \boldsymbol{P}_{\text{cr}} \begin{cases} = 0 & \text{bifurcation point} \\ \neq 0 & \text{limit point} \end{cases} \tag{7}$$

A schematic non-linear load–displacement curve $\lambda P_0 - u$ with corresponding eigenvalue-displacement curves $\Lambda(\lambda P_0) - u$ and $\omega - u$ are depicted in Figure 1, see black, red and blue curve, respectively.

For some structures, a linear pre-buckling behavior can be observed. In such cases, only a single linear calculation step and the solution of an eigenvalue problem are required. This motivates the use of the linear buckling analysis as a special case of the non-linear analysis. It starts from the displacement state $\boldsymbol{u} = \boldsymbol{0}$, where the linear solution

$$\boldsymbol{K}_T(\boldsymbol{0})\boldsymbol{u}_0 = \boldsymbol{P}_0 \quad \Leftrightarrow \quad \boldsymbol{u}_0 = \boldsymbol{K}_T^{-1}(\boldsymbol{0})\boldsymbol{P}_0 \tag{8}$$

is computed for an external basic load of $\boldsymbol{P}_0$ ($\lambda_0 = 1$) with $\boldsymbol{K}_T(\boldsymbol{0}) = \boldsymbol{K}_{\text{lin}}$. Thus, the linear buckling analysis is defined as

$$[\boldsymbol{K}_{\text{lin}} + \Lambda_0 \boldsymbol{K}_{\text{nlin}}(\boldsymbol{u}_0)]\, \boldsymbol{\varphi}_0 = \boldsymbol{0} \tag{9}$$

The associated critical load and displacement vectors are

$$\tilde{\boldsymbol{P}}_{\text{cr}} = \boldsymbol{P}_{\text{cr,lin}} = \Lambda_0 \boldsymbol{P}_0 \tag{10}$$

$$\tilde{\boldsymbol{u}}_{\text{cr}} = \boldsymbol{u}_{\text{cr,lin}} = \Lambda_0 \boldsymbol{u}_0 \tag{11}$$

However, as shown in Figure 1, the results of a linear buckling analysis (maximum value of the green curve) can significantly differ from the non-linear buckling load (maximum value of the black curve) in the case of non-linear pre-buckling behavior. This requires a comprehensive geometrically non-linear path-following analysis using an iterative procedure such as the Newton-Raphson scheme. In this paper, the non-linear buckling analysis is performed by a path-following analysis, where the signs of the diagonal elements of the tangent stiffness matrix are observed. A change in the sign of the diagonal elements of $\boldsymbol{K}_T$ indicates a change in the equilibrium state, with

$$\begin{aligned} &\forall D_{ii}\ ,\ D_{ii} > 0 \rightarrow \text{stable} \\ &\exists D_{ii}\ ,\ D_{ii} = 0 \rightarrow \text{indifferent, (stability point)} \\ &\exists D_{ii}\ ,\ D_{ii} < 0 \rightarrow \text{unstable} \end{aligned} \tag{12}$$

If at least one of the diagonal elements D_{ii} becomes negative, the calculation is terminated and the load state is saved. At this equilibrium state, the critical load vector $\boldsymbol{P}_{\text{cr}}$ and the initial post-buckling mode $\boldsymbol{\varphi}_{\text{cr}}$ can be computed with the non-linear

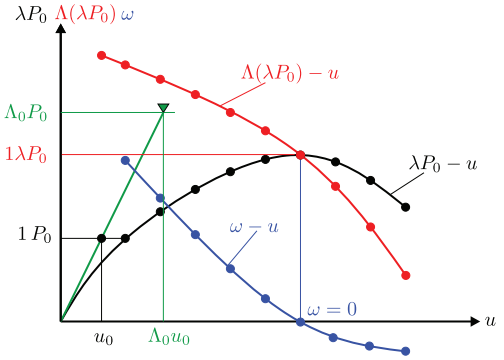

FIGURE 1 | Schematic representation of linear and non-linear buckling analysis.

eigenvalue problem given by Equation (1). Based on the special loading conditions in the examples, the buckling loads P_{cr} and $\tilde{P}_{\text{cr}}$ can be computed from the associated load vectors $\boldsymbol{P}_{\text{cr}}$ and $\tilde{\boldsymbol{P}}_{\text{cr}}$.

3 | Second-Order Statistics of Buckling Load

3.1 | Uncertainty in Buckling Load

The behavior of structures prone to buckling may be affected by several factors, which cannot be quantified deterministically. For example, there may be imperfections in the shells with respect to their nominal dimensions due to uncertainty associated with the manufacturing processes. Also, parameters such as Young's modulus or Poisson's ratio may be affected by uncertainties due to variability associated with batches of raw material. Therefore, these sources of uncertainty must be explicitly accounted for such that their effect can be properly quantified. In the following, it is assumed that the material and geometrical properties of a structure are collected in the vector $\boldsymbol{\xi}$. The uncertainty associated with $\boldsymbol{\xi}$ is characterized by a random variable vector $\boldsymbol{\Xi}$ with probability density function $p_{\boldsymbol{\Xi}}(\boldsymbol{\xi})$ [27]. As the buckling load of a structure P_{cr} depends on the properties of the structure $\boldsymbol{\xi}$, which are assumed to be uncertain, it is clear that the buckling load becomes uncertain as well. In other words, the buckling load P_{cr} is a random variable, with its own probability density function. Calculating the probability density function associated with the buckling load may be challenging for problems of engineering interest, particularly in the tails of the distribution. However, the calculation of second-order statistics (i.e., mean and variance) may be more tractable while still providing valuable insights on the uncertainty associated with the buckling load.

3.2 | Estimation of Second-Order Statistics of Buckling Loads by Means of Monte Carlo Simulation

Recall that the non-linear buckling load P_{cr} depends on the properties of the structure $\boldsymbol{\xi}$. For cases of practical interest, there exists no closed-form relation between the model properties and buckling load. Rather, they must be derived from an FE analysis. As such, an analysis is usually only available in the form of a black-box. That is, for a given input $\boldsymbol{\xi}$, one obtains the output P_{cr}. In this context, Monte Carlo simulation appears as a natural alternative for computing the sought second-order statistics, see, for example, [28]. In a nutshell, a Monte Carlo simulation consists of generating n independent samples $\boldsymbol{\xi}^{(j)},\ j = 1, \ldots, n$ of the properties of the structure distributed according to $p_{\boldsymbol{\Xi}}(\boldsymbol{\xi})$. Then, the buckling loads for each of the samples are calculated, yielding $P_{\text{cr}}\left(\boldsymbol{\xi}^{(j)}\right),\ j = 1, \ldots, n$. Under the assumption that the samples of the properties $\boldsymbol{\xi}^{(j)},\ j = 1, \ldots, n$ are grouped in matrix $\boldsymbol{\Xi}_n$, estimates of the mean value $\widehat{\mu_1'}(P_{\text{cr}}, \boldsymbol{\Xi}_n)$ and the variance $\widehat{\mu_2}(P_{\text{cr}}, \boldsymbol{\Xi}_n)$ are obtained by the following expressions

$$\widehat{\mu_1'}(P_{\text{cr}}, \boldsymbol{\Xi}_n) = \frac{1}{n}\sum_{j=1}^{n} P_{\text{cr}}(\boldsymbol{\xi}^{(j)}) \tag{13}$$

$$\widehat{\mu_2}(P_{\text{cr}}, \boldsymbol{\Xi}_n) = \frac{1}{n-1}\sum_{j=1}^{n} (P_{\text{cr}}(\boldsymbol{\xi}^{(j)}) - \widehat{\mu_1'}(P_{\text{cr}}, \boldsymbol{\Xi}_n))^2 \tag{14}$$

As these estimates are produced by Monte Carlo simulations, they are affected by inherent randomness associated with the sampling process. A means to quantify the quality of these estimates is by calculating their respective variances $\widehat{\sigma^2}[\cdot]$, see, for example, [29],

$$\widehat{\sigma^2}\left[\widehat{\mu_1'}\left(P_{\text{cr}}, \boldsymbol{\Xi}_n\right)\right] = \frac{\widehat{\mu_2}\left(P_{\text{cr}}, \boldsymbol{\Xi}_n\right)}{n} \tag{15}$$

$$\widehat{\sigma^2}\left[\widehat{\mu_2}\left(P_{\text{cr}}, \boldsymbol{\Xi}_n\right)\right] = \frac{\widehat{\mu_4}\left(P_{\text{cr}}, \boldsymbol{\Xi}_n\right)}{n} - \frac{(n-3)\widehat{\mu_2^2}\left(P_{\text{cr}}, \boldsymbol{\Xi}_n\right)}{(n-1)n} \tag{16}$$

In the last equation, $\widehat{\mu_4}\left(P_{\text{cr}}, \boldsymbol{\Xi}_n\right)$ denotes the estimator of the fourth-order central moment of the non-linear buckling load. It is estimated using Equation (A2) in Appendix A.

Equations (15) and (16) indicate that the variances of the estimators for the second-order statistics depend on the number of samples n. It is desirable that these variances are as small as possible, as this increases the confidence that the quantities being estimated are good approximations of the exact second-order statistics. In other words, it is desirable to obtain estimates of these statistics with sufficient *precision*. However, small variances (or equivalently, high precision) may entail a large number of simulations n, which can be quite costly from a numerical viewpoint, as it implies performing n non-linear buckling analyses. Therefore, in practical applications, it is expected that n is actually small and therefore, the estimators will possess large variability. Such a concept is illustrated schematically in Figure 2, where the probability density associated with an estimator $\hat{\mu}$ (which represents either mean or variance, see red curve) is relatively flat, reflecting high uncertainty on the true value of the sought statistic.

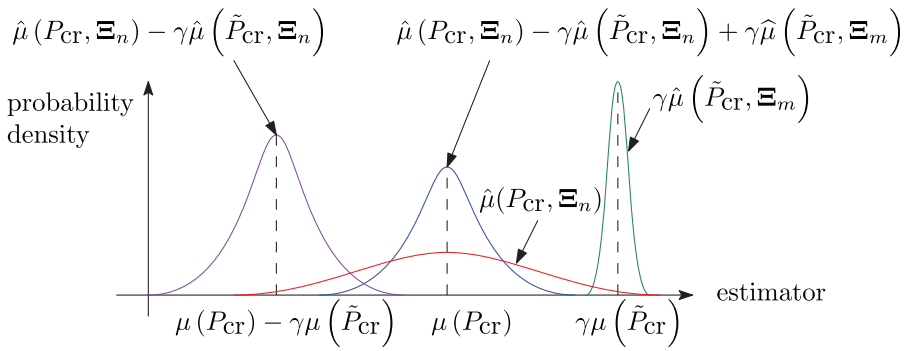

FIGURE 2 | Schematic representation of Control Variates estimator.

4 | Control Variates: A Tool for Aggregating Estimates of Non-Linear and Linear Buckling Analyses

4.1 | Control Variates

The objective is to estimate the second-order statistics of the non-linear buckling load of a structural system. Estimating these statistics with sufficient precision by means of a Monte Carlo simulation may demand a considerable number of non-linear buckling analyses. However, from the discussion in Section 2, it is known that calculating linear buckling loads is numerically less demanding than its non-linear counterpart, although it leads to different values of the sought buckling load. A natural question in this scenario is: Is it possible to leverage linear analysis to estimate statistics of the non-linear buckling load? The answer to this question is affirmative, as this can be carried out within the framework of Control Variates [28, 30]. Indeed, let μ denote a statistic, which can represent either the mean μ_1' or the variance μ_2. Then, the estimator of μ considering Control Variates (CV) is the following:

$$\hat{\mu}^{(\mathrm{CV})} = \hat{\mu}(P_{\mathrm{cr}}, \Xi_n) - \gamma\hat{\mu}(\tilde{P}_{\mathrm{cr}}, \Xi_n) + \gamma\hat{\mu}(\tilde{P}_{\mathrm{cr}}, \Xi_m) \tag{17}$$

In the above equation, Ξ_n and Ξ_m denote two sets with n and m samples, respectively; γ is the so-called *control parameter*, which is actually a real number whose calculation is discussed later on; and $\hat{\mu}(x, \Xi_y)$ denotes estimation of the statistics μ considering the response x (where x could represent either the non-linear or linear buckling load) and Ξ_y denotes a sample set (where y could represent either n or m). It is assumed that $m > n$. The idea behind the Control Variates estimator in Equation (17) is the following.

- The last term $\gamma\hat{\mu}(\tilde{P}_{\mathrm{cr}}, \Xi_m)$ denotes the sought statistic calculated considering the linear buckling load employing a large number of samples m, which is moreover amplified by γ. This last term by itself does not lead to the sought statistic because it involves the linear buckling load (amplified by γ) instead of its non-linear counterpart. However, as m is large, this estimator should possess a relatively low variance. This is illustrated schematically in Figure 2, where the probability density associated with this estimator (shown with the green line) is quite peaked.
- The difference $\hat{\mu}(P_{\mathrm{cr}}, \Xi_n) - \gamma\hat{\mu}(\tilde{P}_{\mathrm{cr}}, \Xi_n)$ in Equation (17) can be interpreted as a correction term, as it subtracts the value of the statistic associated with the linear buckling load amplified by γ and adds the statistic calculated with the non-linear buckling load. Usually, the variance of this difference should be relatively small, even if n itself is small. The reason is that, while the linear and non-linear buckling loads produce different results, it is nevertheless expected that there is a high degree of correlation between them. The probability density associated with this difference is represented schematically with a violet line in Figure 2.

The summation of the two terms described above leads to the Control Variates estimator of Equation (17). In essence, such an estimator allows one to *aggregate* the results stemming from linear and non-linear buckling analyses but still leads to conclusions about the non-linear buckling load. In fact, the effect of the linear buckling load cancels out from Equation (17), as the subtraction between the second and third terms of the right-hand side of that equation is equal to zero. But in that process, the presence of those second and third terms helps in decreasing the variance of the statistics of the buckling load. Indeed, this estimator usually possesses a relatively small variance, as illustrated schematically in Figure 2 with the probability density function in blue color.

The advantage of the Control Variates estimator is that in the calculation process, correlations between linear and non-linear buckling loads are exploited. This implies that the information retrieved from linear buckling analyses may improve the conclusions drawn with respect to non-linear buckling analyses. In this sense, the aforementioned control parameter γ plays a key role. To understand this concept, it is essential to study the variance of the Control Variates estimator. It can be shown that the variance $\hat{\sigma}^2$ associated with the Control Variates estimator is equal to [28]:

$$\begin{aligned}\hat{\sigma}^2\left[\hat{\mu}^{(\mathrm{CV})}\right] = {} & \hat{\sigma}^2\left[\hat{\mu}\left(P_{\mathrm{cr}}, \Xi_n\right)\right] - 2\gamma\hat{\delta}\left[\hat{\mu}\left(P_{\mathrm{cr}}, \Xi_n\right), \hat{\mu}\left(\tilde{P}_{\mathrm{cr}}, \Xi_n\right)\right] \\ & + \gamma^2\hat{\sigma}^2\left[\hat{\mu}\left(\tilde{P}_{\mathrm{cr}}, \Xi_n\right)\right] + \gamma^2\hat{\sigma}^2\left[\hat{\mu}\left(\tilde{P}_{\mathrm{cr}}, \Xi_m\right)\right]\end{aligned} \tag{18}$$

where $\hat{\delta}[\cdot, \cdot]$ denotes the covariance estimator between the arguments. It is noted that the variance of the Control Variates estimator as shown in Equation (18) is a quadratic function with respect to the control parameter γ. Therefore, γ can be selected such that this variance is minimized, which implies forcing the derivative of Equation (18) with respect to γ to be equal to zero. In such way, one determines the optimal control parameter γ^*, which is equal to:

$$\gamma^* = \frac{\hat{\delta}\left[\hat{\mu}\left(P_{\mathrm{cr}}, \Xi_n\right), \hat{\mu}\left(\tilde{P}_{\mathrm{cr}}, \Xi_n\right)\right]}{\hat{\sigma}^2\left[\hat{\mu}\left(\tilde{P}_{\mathrm{cr}}, \Xi_n\right)\right] + \hat{\sigma}^2\left[\hat{\mu}\left(\tilde{P}_{\mathrm{cr}}, \Xi_m\right)\right]} \tag{19}$$

In summary, the application of Equations (17), (18), and (19) allows estimating the sought statistic (either mean or variance) by means of Control Variates. These equations are applied in the following order. First, the buckling loads considering linear ($\tilde{P}_{\mathrm{cr}}$) and non-linear analysis (P_{cr}) are calculated for each sample contained in the set Ξ_n. In addition, the buckling loads considering linear analysis only are evaluated for each sample contained in the set Ξ_m. Considering all of these samples, Equation (19) is evaluated to obtain the optimal control parameter γ^*. This optimal control parameter is then used together with the samples of the buckling loads associated with the sets Ξ_n and Ξ_m to evaluate the sought statistic through Equation (17) as well as the variance of this estimator by means of Equation (18).

As noted from the above description, the application of Control Variates is completely non-intrusive. That is, it is not necessary to access to system's matrices. It just suffices to conduct linear and non-linear buckling analyses for different sets of samples. Then, the Control Variates estimate in Equation (17) merges the information contained in these samples to produce an estimate of the sought statistic involving non-linear buckling analysis. Indeed, the role of the samples of the linear buckling load in the estimator is simply to exploit correlations to reduce the variance of the estimator of the sought statistic. In that sense, the optimal control parameter γ^* in Equation (19) plays a pivotal role. To understand its role better, consider the case where there is a high covariance between buckling loads calculated using linear and non-linear

buckling analysis. In such a situation, performing linear buckling analysis is almost *as good as* performing non-linear buckling analysis, meaning that both types of analyses are capable of uncovering the effects of uncertainty in the buckling load. In such a situation of high covariance, the control parameter $\gamma^\star$ will naturally approach to 1 and thus, the Control Variates estimator provides more importance to the information carried by the samples of the linear buckling load, which translates into an estimator of the sought statistic with reduced variance. In the (unlikely) event that the covariance $\widehat{\delta}$ between the linear and non-linear buckling load is zero, the control parameter itself becomes zero and the estimator of Equation (17) reduces to its plain Monte Carlo counterpart. In such a case, as there is no covariance $\widehat{\delta}$, the Control Variates estimate cannot leverage on the information carried by the samples of the linear buckling load and therefore, the sought estimate is produced based on the samples of the non-linear buckling analysis only.

To summarize the concepts described above, the application of Control Variates for estimating buckling loads can be visualized as follows. First, a relatively small number of samples of the buckling load are generated considering non-linear buckling analysis. As the number of samples drawn is small, the estimators drawn out of those samples (such as mean and variance) will be most likely highly uncertain (implying that their variances are high). But then, if one performs additional sampling using linear buckling analyses, it is possible to exploit covariance between linear and non-linear buckling analyses to reduce the variance of the estimators associated with the non-linear buckling load.

4.2 | Control Variates With Splitting

The previous section has presented the application of the Control Variates framework. For its practical implementation, note that the same samples of the linear and non-linear buckling load are used for both evaluating the optimal control parameter (see Equation (19)) and the sought statistic (see Equation (17)). However, such a strategy induces bias in the estimator of the statistic, as documented, for example, in Reference [30]. The effect of bias can be particularly notorious in the case that the sample set $\boldsymbol{\Xi}_n$ possesses a small number n of samples, which is expected to be precisely the case in practical applications, because performing n non-linear buckling analyses is numerically demanding. A remedy to eliminate bias is to resort to a *Splitting* approach, as proposed in Reference [19]. This is quite a convenient scheme, as it does not demand performing additional buckling analyses (neither linear nor non-linear). The splitting approach consists of dividing the set of available samples into subsets. Then, the associated estimators (for example, mean, variance, optimal control parameter) are estimated for each of these subsets. Finally, the estimators for the subsets are aggregated in such a way that bias is effectively eliminated. As discussed in Reference [19], the number of subsets to be considered should be equal to or larger than 3. However, a large number of subsets may increase the variance. Therefore, in this paper, a minimum of 3 subsets is considered to implement the splitting approach.

How does the splitting approach work in practice? First, each of the sample sets $\boldsymbol{\Xi}_n$ and $\boldsymbol{\Xi}_m$ is partitioned into three subsets $\boldsymbol{\Xi}_{m^*,k}$ and $\boldsymbol{\Xi}_{n^*,k}$, where $k = 1, 2, 3$ and $n^* = n/3$ and $m^* = m/3$. Here, it is implicitly assumed that n and m are selected such that they are multiples of 3. For each subset k, the subset controller $\tau(k)$ is defined [19], as shown in Table 1.

Once the subsets have been defined, the expressions for calculating the sought statistic, its variance, and the optimal control parameter by means of Control Variates with Splitting (CV+S) are:

$$\widehat{\mu}^{(\mathrm{CV+S})} = \frac{1}{3}\sum_{k=1}^{3} \widehat{\mu}(P_{\mathrm{cr}}, \boldsymbol{\Xi}_{n^*,k}) - \gamma_{\tau(k)}\widehat{\mu}(\tilde{P}_{\mathrm{cr}}, \boldsymbol{\Xi}_{n^*,k}) + \gamma_{\tau(k)}\widehat{\mu}(\tilde{P}_{\mathrm{cr}}, \boldsymbol{\Xi}_{m^*,k}) \tag{20}$$

$$\begin{aligned}\widehat{\sigma}^2\left[\widehat{\mu}^{(\mathrm{CV+S})}\right] = \frac{1}{3^2}\sum_{k=1}^{3} &\widehat{\sigma}^2\left[\widehat{\mu}\left(P_{\mathrm{cr}}, \boldsymbol{\Xi}_{n^*,k}\right)\right] \\ &- 2\gamma^*_{\tau(k)}\widehat{\delta}\left[\widehat{\mu}\left(P_{\mathrm{cr}}, \boldsymbol{\Xi}_{n^*,k}\right), \widehat{\mu}\left(\tilde{P}_{\mathrm{cr}}, \boldsymbol{\Xi}_{n^*,k}\right)\right] \\ &+ \left(\gamma^*_{\tau(k)}\right)^2\widehat{\sigma}^2\left[\widehat{\mu}\left(\tilde{P}_{\mathrm{cr}}, \boldsymbol{\Xi}_{n^*,k}\right)\right] \\ &+ \left(\gamma^*_{\tau(k)}\right)^2\widehat{\sigma}^2\left[\widehat{\mu}\left(\tilde{P}_{\mathrm{cr}}, \boldsymbol{\Xi}_{m^*,k}\right)\right]\end{aligned} \tag{21}$$

$$\gamma^*_{\tau(k)} = \frac{\widehat{\delta}\left[\widehat{\mu}\left(P_{\mathrm{cr}}, \boldsymbol{\Xi}_{n^*,\tau(k)}\right), \widehat{\mu}\left(\tilde{P}_{\mathrm{cr}}, \boldsymbol{\Xi}_{n^*,\tau(k)}\right)\right]}{\widehat{\sigma}^2\left[\widehat{\mu}\left(\tilde{P}_{\mathrm{cr}}, \boldsymbol{\Xi}_{n^*,\tau(k)}\right)\right] + \widehat{\sigma}^2\left[\widehat{\mu}\left(\tilde{P}_{\mathrm{cr}}, \boldsymbol{\Xi}_{m^*,\tau(k)}\right)\right]}, \quad k = 1, 2, 3 \tag{22}$$

The structure of Equations (20), (21), and (22) reveals the essence of the Splitting approach. That is, when applying Control Variates to calculate either the estimator of the sought statistic (see Equation (20)) or its variance (see Equation (21)), one considers the k-th subset of samples for calculating $\widehat{\mu}$ while the optimal control parameter is calculated using the $\tau(k)$-th subset of samples. As $k \neq \tau(k)$, such a strategy effectively ensures that bias is avoided, as demonstrated in detail in Reference [19]. Furthermore, it is noted from Equations (20), (21), and (22) that the implementation of the Splitting strategy does not demand any additional buckling analyses. Instead, it demands performing calculations of the different estimators and optimal control parameters over different subsets, which is quite cheap from a numerical viewpoint. In summary, the Splitting technique offers a convenient way to avoid the undesirable effects of bias while not increasing numerical costs.

4.3 | Estimation of the Mean

The preceding section illustrates how a statistic of interest μ is estimated by means of Control Variates with Splitting, where μ can represent either mean or variance. When the focus is on estimating the mean of the non-linear buckling load (denoted as $\widehat{\mu_1'}^{(\mathrm{CV+S})}$) by means of Control Variates with Splitting as well as

TABLE 1 | Subset controllers $\tau(k)$ for each subset k.

Subset k	Subset controller $\tau(k)$
1	2
2	3
3	1

the variance of that estimator (i.e., $\widehat{\sigma}^2\left[\widehat{\mu_1'}^{(\mathrm{CV+S})}\right]$), Equations (20), (21), and (22) adopt the following specific form, respectively

$$\widehat{\mu_1'}^{(\mathrm{CV+S})} = \frac{1}{3}\sum_{k=1}^{3}\widehat{\mu_1'}(P_{\mathrm{cr}}, \Xi_{n^*,k}) - \alpha_{\tau(k)}\widehat{\mu_1'}(\tilde{P}_{\mathrm{cr}}, \Xi_{n^*,k}) + \alpha_{\tau(k)}\widehat{\mu_1'}(\tilde{P}_{\mathrm{cr}}, \Xi_{m^*,k}) \tag{23}$$

$$\begin{aligned}\widehat{\sigma}^2\left[\widehat{\mu_1'}^{(\mathrm{CV+S})}\right] = \frac{1}{3^2}\sum_{k=1}^{3}&\frac{\widehat{\mu_{2,0}}(P_{\mathrm{cr}}, \tilde{P}_{\mathrm{cr}}, \Xi_{n^*,k})}{n^*} - 2\alpha^*_{\tau(k)}\frac{\widehat{\mu_{1,1}}(P_{\mathrm{cr}}, \tilde{P}_{\mathrm{cr}}, \Xi_{n^*,k})}{n^*} \\ &+ \left(\alpha^*_{\tau(k)}\right)^2\frac{\widehat{\mu_{0,2}}(P_{\mathrm{cr}}, \tilde{P}_{\mathrm{cr}}, \Xi_{n^*,k})}{n^*} + \left(\alpha^*_{\tau(k)}\right)^2\frac{\widehat{\mu_{0,2}}(P_{\mathrm{cr}}, \tilde{P}_{\mathrm{cr}}, \Xi_{m^*,k})}{m^*}\end{aligned} \tag{24}$$

$$\alpha^*_{\tau(k)} = \frac{\frac{\widehat{\mu_{1,1}}(P_{\mathrm{cr}}, \tilde{P}_{\mathrm{cr}}, \Xi_{n^*,\tau(k)})}{n^*}}{\frac{\widehat{\mu_{0,2}}(P_{\mathrm{cr}}, \tilde{P}_{\mathrm{cr}}, \Xi_{n^*,\tau(k)})}{n^*} + \frac{\widehat{\mu_{0,2}}(P_{\mathrm{cr}}, \tilde{P}_{\mathrm{cr}}, \Xi_{m^*,\tau(k)})}{m^*}}, \quad k = 1, 2, 3 \tag{25}$$

In the above equations, $\widehat{\mu_1'}$ refers to the estimator of the mean (see Equation (13)); $\alpha^*_{\tau(k)}$ represents the optimal control parameter associated the $\tau(k)$-th subset which is related with the estimation of the mean; and the term $\widehat{\mu_{p,q}}$ represents the estimator of the bivariate central co-moment of order (p, q) between the non-linear and linear buckling loads. Detailed expressions for evaluating these co-moments are listed in Appendix A.

4.4 | Estimation of the Variance

When the objective is to estimate the variance of the buckling load (denoted as $\widehat{\mu_2}^{(\mathrm{CV+S})}$) as well as the variance of that estimator (represented as $\widehat{\sigma}^2\left[\widehat{\mu 2}^{(\mathrm{CV+S})}\right]$) by means of Control Variates with Splitting, Equations (20), (21), and (22) must be formulated as

$$\widehat{\mu_2}^{(\mathrm{CV+S})} = \frac{1}{3}\sum_{k=1}^{3}\widehat{\mu_2}(P_{\mathrm{cr}}, \Xi_{n^*,k}) - \beta_{\tau(k)}\widehat{\mu_2}(\tilde{P}_{\mathrm{cr}}, \Xi_{n^*,k}) + \beta_{\tau(k)}\widehat{\mu_2}(\tilde{P}_{\mathrm{cr}}, \Xi_{m^*,k}) \tag{26}$$

$$\begin{aligned}\widehat{\sigma}^2\left[\widehat{\mu 2}^{(\mathrm{CV+S})}\right] = \frac{1}{3^2}\sum_{k=1}^{3}&B_1\left(P_{\mathrm{cr}}, \tilde{P}_{\mathrm{cr}}, \Xi_{n^*,k}\right) - 2\beta_{\tau(k)}B_2\left(P_{\mathrm{cr}}, \tilde{P}_{\mathrm{cr}}, \Xi_{n^*,k}\right) \\ &+ \left(\beta_{\tau(k)}\right)^2 B_3\left(P_{\mathrm{cr}}, \tilde{P}_{\mathrm{cr}}, \Xi_{n^*,k}\right) + \left(\beta_{\tau(k)}\right)^2 B_4\left(P_{\mathrm{cr}}, \tilde{P}_{\mathrm{cr}}, \Xi_{m^*,k}\right)\end{aligned} \tag{27}$$

$$\beta^*_{\tau(k)} = \frac{B_2\left(P_{\mathrm{cr}}, \tilde{P}_{\mathrm{cr}}, \Xi_{n^*,\tau(k)}\right)}{B_3\left(P_{\mathrm{cr}}, \tilde{P}_{\mathrm{cr}}, \Xi_{n^*,\tau(k)}\right) + B_4\left(P_{\mathrm{cr}}, \tilde{P}_{\mathrm{cr}}, \Xi_{m^*,\tau(k)}\right)}, \quad k = 1, 2, 3 \tag{28}$$

In the last three equations, $\widehat{\mu_2}$ represents the estimator of the variance (see Equation (14)); $\beta^*_{\tau(k)}$ is the optimal control parameter associated with the $\tau(k)$-th subset which is related with the estimation of the variance; and B_1, B_2, B_3 and B_4 are real constants that are calculated by:

$$B_1\left(P_{\mathrm{cr}}, \tilde{P}_{\mathrm{cr}}, \Xi_{n^*,k}\right) = \frac{\widehat{\mu_{4,0}}\left(P_{\mathrm{cr}}, \tilde{P}_{\mathrm{cr}}, \Xi_{n^*,j}\right)}{n^*} - \frac{(n^*-3)}{(n^*-1)n^*}\widehat{\mu^2_{2,0}}\left(P_{\mathrm{cr}}, \tilde{P}_{\mathrm{cr}}, \Xi_{n^*,k}\right) \tag{29}$$

$$B_2\left(P_{\mathrm{cr}}, \tilde{P}_{\mathrm{cr}}, \Xi_{n^*,k}\right) = \frac{2\widehat{\mu^2_{1,1}}\left(P_{\mathrm{cr}}, \tilde{P}_{\mathrm{cr}}, \Xi_{n^*,k}\right)}{(n^*-1)n^*} + \frac{\widehat{\mu_{2,2}}\left(P_{\mathrm{cr}}, \tilde{P}_{\mathrm{cr}}, \Xi_{n^*,k}\right)}{n^*} - \frac{\widehat{\mu_{2,0}\mu_{0,2}}\left(P_{\mathrm{cr}}, \tilde{P}_{\mathrm{cr}}, \Xi_{n^*,k}\right)}{n^*} \tag{30}$$

$$B_3\left(P_{\mathrm{cr}}, \tilde{P}_{\mathrm{cr}}, \Xi_{n^*,k}\right) = \frac{\widehat{\mu_{0,4}}\left(P_{\mathrm{cr}}, \tilde{P}_{\mathrm{cr}}, \Xi_{n^*,j}\right)}{n^*} - \frac{(n^*-3)}{(n^*-1)n^*}\widehat{\mu^2_{0,2}}\left(P_{\mathrm{cr}}, \tilde{P}_{\mathrm{cr}}, \Xi_{n^*,k}\right) \tag{31}$$

$$B_4\left(P_{\mathrm{cr}}, \tilde{P}_{\mathrm{cr}}, \Xi_{m^*,k}\right) = \frac{\widehat{\mu_{0,4}}\left(P_{\mathrm{cr}}, \tilde{P}_{\mathrm{cr}}, \Xi_{m^*,k}\right)}{m^*} - \frac{(m^*-3)}{(m^*-1)m^*}\widehat{\mu^2_{0,2}}\left(P_{\mathrm{cr}}, \tilde{P}_{\mathrm{cr}}, \Xi_{m^*,k}\right) \tag{32}$$

Expressions for evaluating the co-moments associated with the calculation of constants B_1, B_2, B_3, and B_4 can be found in Appendix A.

5 | Numerical Examples

Three numerical examples are presented using geometric non-linear quadrilateral shell elements with moderate rotations, as described in Reference [31]. This four-node element is based on the isoparametric concept with linear shape functions. To prevent shear locking, the assumed natural strain (ANS) method is implemented. The element is incorporated into an extended version of the general finite element analysis program (FEAP) [32]. An interface has been developed to enable FEAP to be called from MATLAB, allowing the calculation of buckling load solutions within the Monte Carlo loop.

The linear buckling analysis is performed using the subspace iteration method as described in References [33, 34]. In Reference [33], the recommended number of eigenvalues to be determined by iteration is given by $N = \min\{2\,n, n+8\}$, where n is the number of desired eigenvalues. The first eigenvalue indicates the stability point. Therefore, n is set to one to maximize the performance of the Control Variates approach. To compare the speed-up factors between the Control Variates approach and the Monte Carlo simulation for the presented examples, all calculations are performed on the same workstation with the following setup: 2 × CPUs Intel Xeon E5-2667 v4 8 cores @ 3.20 GHz, 128 GB RAM, Win 10 ×64.

5.1 | Folded Plate

The first example of a folded plate, as depicted in Figure 3, is to show that the Control Variates method works successfully in the presence of two types of stability points: bifurcation points and a limit point (snap-through).

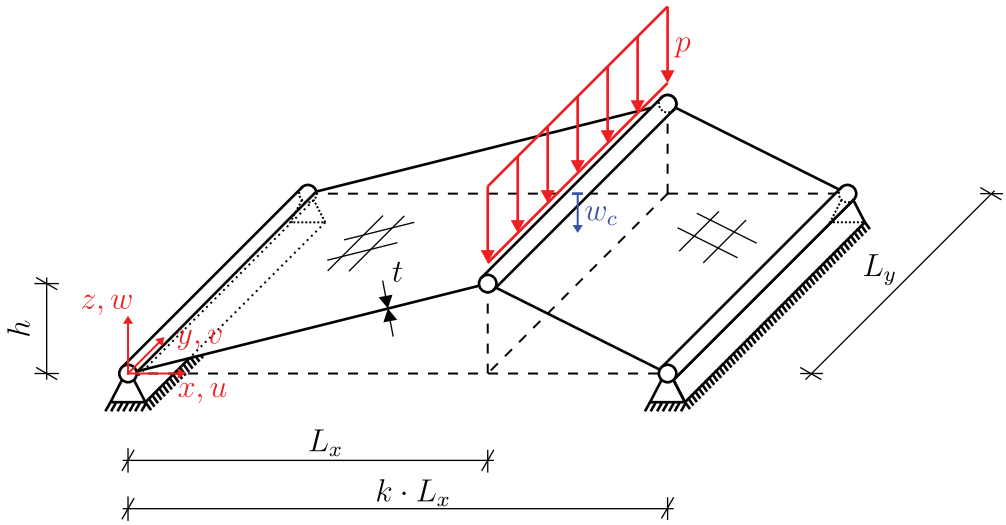

FIGURE 3 | Folded Plate subjected to a distributed load.

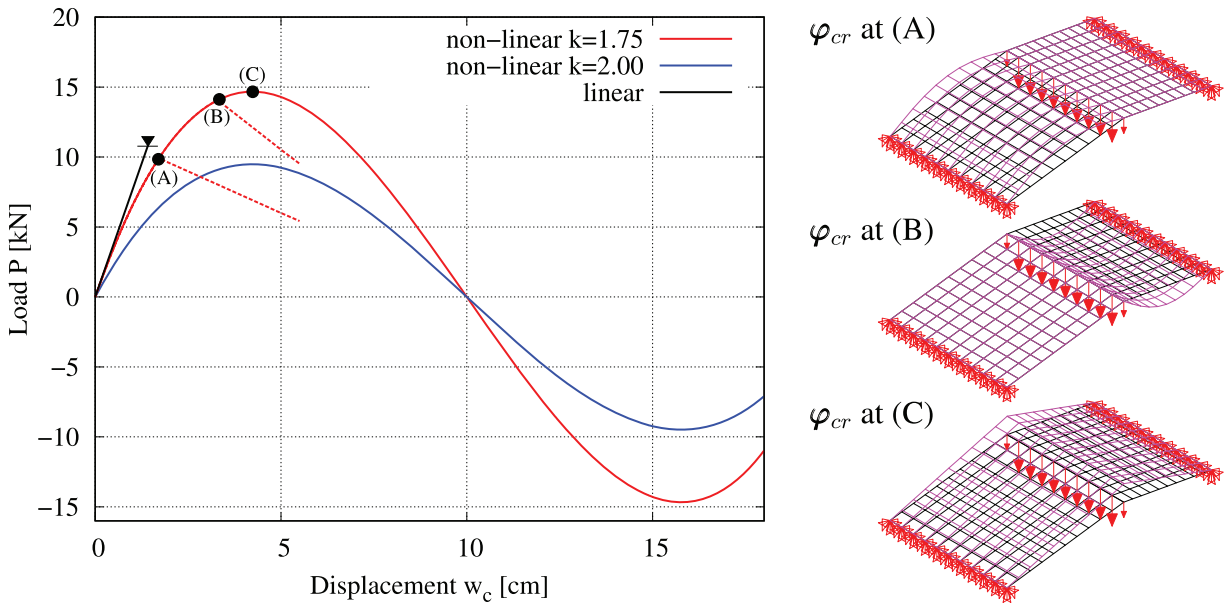

FIGURE 4 | Load–displacement curves of the folded plate.

A distributed load p is applied to the plate at the hinged sleeve along the line $x = L_x$. The folded plate is simply supported at the edges $x = 0$ and $x = k \cdot L_x$, with boundary conditions $u = v = w = 0$. The lengths L_x and L_y are set to 100 cm and the plate thickness is defined as $t = 5$ cm. A length factor k allows for control of the symmetry of the system and thus also the buckling behavior. For $k = 1.75$, the system is non-symmetric, whereas a symmetric system occurs when $k = 2.00$. For an initial analysis, the Young's modulus is set to $E = 1,000\,\text{kN/cm}^2$ and the height to $h = 10$ cm. Each subarea to the left and right of the hinged sleeve is discretized with 10×10 elements. The vertical displacements of all nodes of the hinged sleeve are linked. The resulting load $P = p\,L_y$ is computed for an increasing vertical displacement w_c at $x = L_x$, $y = L_y/2$ using the arc-length method with a displacement control of $\Delta w = 0.02$ cm. The resulting load–displacement curve for a non-symmetric system ($k = 1.75$) is depicted in Figure 4.

Two bifurcation points (A) and (B) occur before the snap-through point (C). In addition, associated eigenvectors $\boldsymbol{\varphi}_{cr}$ are depicted in Figure 4. The first eigenvectors in points (A) and (B) represent a local buckling of the left or right part of the folded plate, whereas the eigenvectors at point (C) indicate the snap-through as a global buckling failure mode. By applying the corresponding eigenvectors as small imperfections at points (A) and (B), the resulting secondary equilibrium paths, illustrated by the red dashed lines, can be traced. A non-linear buckling analysis yields a buckling load of $P_{cr} = 9.92$ kN at bifurcation point (A), $P_{cr} = 14.07$ kN at point (B) and $P_{cr} = 14.67$ kN at the snap-through point (C). The critical load from the linear buckling analysis is $\tilde{P}_{cr} = 10.83$ kN.

In the following, the length factor k, height h, and Young's modulus E are modeled as truncated Gaussian random variables. Their mean values μ and standard deviations σ are listed in Table 2.

TABLE 2 | Folded plate: Quantification of material and geometric parameters as truncated Gaussian random variables.

Parameter	Mean value μ	Standard deviation σ
length factor k [-]	1.75	0.05
height h [cm]	10	1
Young's modulus E [kN/cm^2]	1000	100

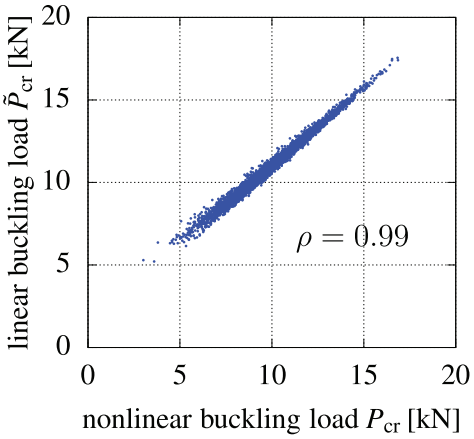

FIGURE 5 | Correlation between buckling loads calculated using non-linear P_{cr} and linear analysis $\tilde{P}_{cr}$.

TABLE 3 | Estimates of second-order statistics for the buckling load of the folded plate.

Approach	Monte Carlo	Control Variates with splitting
n	1,750	150
m	—	3,000
n_e	1,750	736
$\widehat{\mu_1'}$ N	9.99	9.97
$V\left[\widehat{\mu_1'}\right]$ N^2	0.002	0.002
$\delta_{\widehat{\mu_1'}}$	0.45%	0.39%
$\widehat{\mu_2}$ N^2	3.582	3.614
$V\left[\widehat{\mu_2}\right]$ N^4	0.015	0.018
$\delta_{\widehat{\mu_2}}$	3.45%	3.65%
$\delta_{P_{cr}}$	19%	19%

The stochastic non-linear buckling response is analyzed via a Monte Carlo simulation with 5000 samples, resulting in a mean value of the critical buckling load of $\mu_{P_{cr}} = 9.94$ kN and a coefficient of variation of $\delta_{P_{cr}} = 18.82\%$. All buckling loads correspond to the load at which the first diagonal element becomes negative. Despite the significant influence of the three random input parameters defined in Table 2 on the buckling behavior, a strong correlation of $\rho = 0.99$ between the linear and non-linear buckling analysis is evident, see Figure 5. These conditions are well-suited for applying the Control Variates method. The results are given in Table 3.

The estimates obtained using Monte Carlo and Control Variates with Splitting are nearly identical, as indicated by the coefficient of variation δ in Table 3. To compare the numerical efforts between the two approaches for estimating second-order statistics, the total number of analyses performed for Control Variates is expressed as an equivalent number of analyses n_e (relative to plain Monte Carlo simulation). This equivalent number of analyses is calculated by

$$n_e = n + \frac{n+m}{f_s} \tag{33}$$

where n is the number of samples for the non-linear buckling analysis and m is the number of samples for the linear buckling analysis. The factor f_s is defined as the ratio between the execution time of one non-linear buckling analysis and one linear buckling analysis. For this example, the factor is $f_s = 5.38$, indicating that the linear buckling analysis is 5.38 times faster than the non-linear buckling analysis. Thus, the equivalent number of $n_e = 736$ in Table 3 can be calculated, showing that the Control Variates method requires only 736 equivalent simulations instead of 1750 Monte Carlo simulations. Overall, the ratio of the equivalent numbers of the analyses shows that the stochastic buckling analysis using Control Variates is approximately $1750/736 \approx 2.4$ times more efficient than plain Monte Carlo simulation.

Finally, it should be noted that even if a bifurcation path exists in the pre-buckling stage, the method still performs successfully. The only essential requirement is a strong correlation between the linear and non-linear buckling analyses, while the type of stability point plays a subordinate role. If a sufficiently strong correlation exists, the Control Variates method yields reliable results.

5.2 | Composite Shell Panel

This example demonstrates the use of the Control Variates approach to predict buckling loads in a composite shell panel subjected to a single load and random geometric imperfections. For details on the shell panel model, see [35]. Figure 6 illustrates the

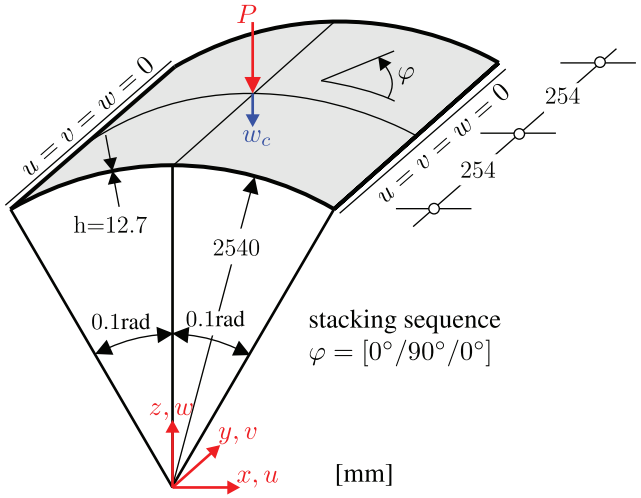

FIGURE 6 | Cylindrical composite shell panel subjected to a single load.

TABLE 4 | Transversal isotropic material properties of the laminate.

E_{11} [N/mm²]	E_{22} [N/mm²]	G_{12} [N/mm²]	G_{13} [N/mm²]	G_{23} [N/mm²]	ν_{12} [-]
3,300	1,100	660	660	450	0.3

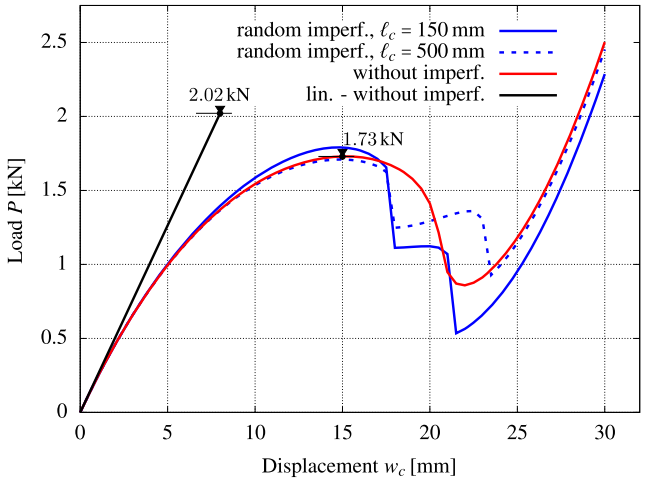

FIGURE 7 | Load–displacement curves of the composite shell panel.

system modeled with a 30×30 FE mesh. The panel is simply supported along the two lateral edges. System symmetry cannot be exploited due to applied random geometrical imperfections.

The transversely isotropic material properties of the laminate are provided in Table 4. The panel consists of a three-layer laminate with a total thickness of $h = 12.7$ mm. The corresponding stacking sequence is given in Figure 6.

First of all, the buckling behavior is analyzed without any imperfections. The load–displacement curves, evaluating the load P vs. the vertical displacement w_c at the center of the panel, are depicted in Figure 7. These curves are obtained using the arc-length method with a displacement control $\Delta w = 0.5$ mm.

A pronounced non-linear pre-buckling behavior is observed. Consequently, the non-linear buckling analysis using the criterion in Equation (12) results in a critical load of $P_{\text{cr}} = 1.73$ kN, while the linear buckling analysis according to Equation (9) yields a higher critical load of $\tilde{P}_{\text{cr}} = 2.02$ kN.

The next step is to generate random geometric imperfections of the cylindrical shell shape (reference surface) modeled as Gaussian random fields using the Karhunen-Loève Expansion (KLE). For the fundamentals of random field modeling, see, for example, [36, 37]. Accordingly, the random geometric deviations in the radial direction of the shell panel can be expressed as

$$\hat{w}_{\text{rad}}(\boldsymbol{x}, \theta) = \mu + \sum_{i=1}^{M} \sqrt{\lambda_i}\, \xi_i(\theta)\, \varphi_i(\boldsymbol{x}) \tag{34}$$

Here, the mean value μ is set to zero to model geometric imperfections that vary around the reference surface. The parameter $\xi_i(\theta)$ is a standard normal distributed random variable, $\boldsymbol{\varphi}_i(\boldsymbol{x})$ are the eigenfunctions and λ_i the eigenvalues of the covariance matrix formulated for the FE mesh with M nodes. This covariance matrix is assumed to be homogeneous

$$C(\tau) = \sigma^2 \rho(\tau) \tag{35}$$

where the variance σ^2 is set to one in this example. The autocorrelation function (acf) $\rho(\tau)$ is defined as a function of the relative distance τ of two FE nodes $\boldsymbol{x}_i$, $\boldsymbol{x}_j$

$$\rho(\boldsymbol{x}_i, \boldsymbol{x}_j) = \rho(\tau) \quad \text{with} \quad \tau = \boldsymbol{x}_j - \boldsymbol{x}_i \tag{36}$$

In practical applications, analytical models for autocorrelation are frequently used [38, 39]. For the presented example, the Whittle–Matérn acf is chosen to generate the shell imperfections

$$\rho(\tau) = \frac{2^{1-\nu}}{\Gamma(\nu)} \left(\sqrt{2\nu} \frac{\tau}{\ell_c} \right)^{\nu} K_{\nu} \left(\sqrt{2\nu} \frac{\tau}{\ell_c} \right) \tag{37}$$

where K_ν is the modified Bessel function of the second kind and $\Gamma(\nu)$ denotes the Gamma function. The parameter ℓ_c is the correlation length and ν is the so-called "smoothness" parameter, which is set to $\nu = 1.5$.

The correlation length influences the imperfection shape, thereby it also influences the buckling behavior and the second-order statistics of the buckling load. Figure 8 illustrates the mean $\mu_{P_{\text{cr}}}$ and the coefficient of variation $\delta_{P_{\text{cr}}}$ of the buckling load as functions of the correlation length.

For the small correlation length $\ell_c = 150$ mm, a minimal mean value of $\mu_{P_{\text{cr}}} = 1.68$ kN and a maximum coefficient of variation of $\delta_{P_{\text{cr}}} = \sigma_{P_{\text{cr}}} / \mu_{P_{\text{cr}}} = 10\%$ can be observed. From this point, the mean value converges to the imperfection-free buckling load $P_{\text{cr}} = 1.73$ kN, and the coefficient of variation decreases. This is because, for large correlation lengths, the effect of geometric imperfections vanishes. Examining the vertical axis of Figure 8 (left), the mean value shows small variation. However, the correlation length has a significant influence on the coefficient of variations, see Figure 8 (right). Therefore, two different correlation lengths are selected to investigate the effectiveness of Control Variates: The smaller length of $\ell_c = 150$ mm, which results in wavy realizations, and a larger length of $\ell_c = 500$ mm, which produces more uniform imperfection shapes as depicted in Figure 9.

In addition, the load–displacement curves for two realizations of the selected correlation lengths are depicted in Figure 7. For these realizations, a small difference in the buckling load can be observed, consistent with the slight deviations in the mean value shown in Figure 8 (left). In Figure 10, the eigenvectors $\boldsymbol{\varphi}_{cr}$ at the stability point are depicted for the panel without and with the imperfection from Figure 9 (left).

The eigenvectors are quite similar. However, the eigenvector with imperfections is non-symmetric, leading to different post-buckling behavior. Table 5 summarizes the second-order

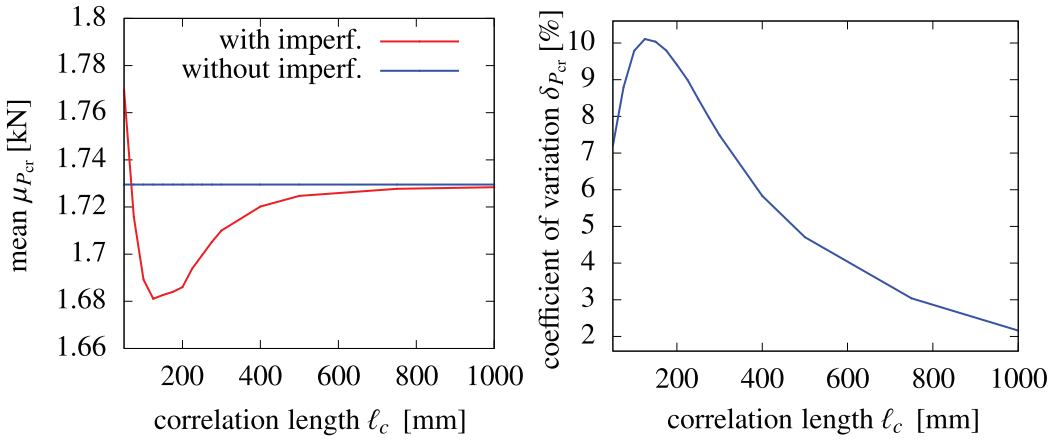

FIGURE 8 | Mean $\mu_{P_{cr}}$ (left) and coefficient of variation $\delta_{P_{cr}}$ (right) of the buckling load as a function of the correlation length.

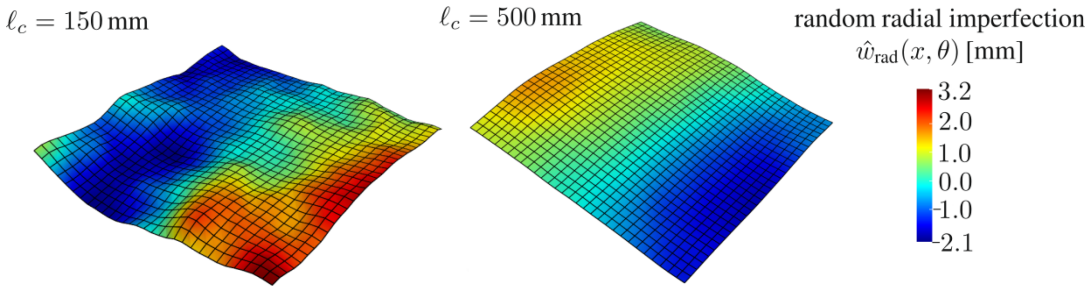

FIGURE 9 | Random geometrical imperfection with respect to the shell surface for $\ell_c = 150\,\text{mm}$ (left) and $\ell_c = 500\,\text{mm}$ (right).

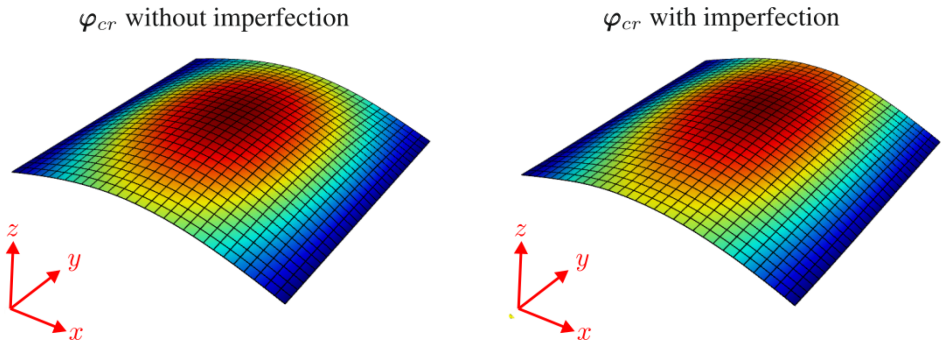

FIGURE 10 | Eigenvectors $\boldsymbol{\varphi}_{cr}$ at the stability point of the shell panel without (left) and realization with random imperfection for the correlation length $\ell_c = 150\,\text{mm}$ (right).

TABLE 5 | Second-order statistics of the buckling load for different correlation lengths.

Correlation length ℓ_c [mm]	$\mu_{P_{cr}}$ [kN]	$\delta_{P_{cr}}$ [%]
150	1.68	10.0
500	1.72	4.7

statistics for both correlation lengths, as evaluated using a Monte Carlo simulation with 5000 realizations.

For instance, Figure 11 shows the Monte Carlo convergence test for generated random imperfections with the correlation length $\ell_c = 150\,\text{mm}$. For 1000 samples, the relative error of $\delta_{P_{cr}}$ compared to the reference solution provided in Table 5 is smaller than 5%.

Figure 12 shows the correlations between buckling loads calculated using non-linear (P_{cr}) and linear analysis ($\tilde{P}_{cr}$) for the small and large correlation length. For each correlation length, 5000 random fields are generated, and the buckling loads with the linear and non-linear buckling analysis are calculated.

It is noteworthy that a strong correlation of $\rho = 0.97$ is observed even for the small correlation length of $\ell_c = 150\,\text{mm}$. Compared to the larger length $\ell_c = 500\,\text{mm}$, the correlation between linear and non-linear buckling analyses decreases only slightly. This is a good condition for using Control Variates. Calculating the

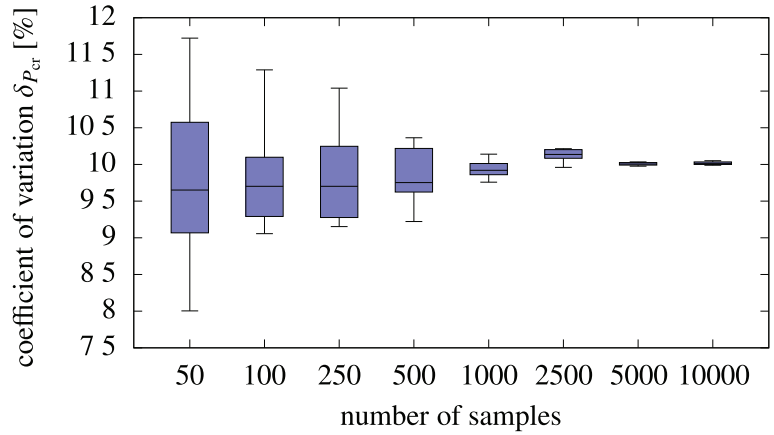

FIGURE 11 | Monte Carlo convergence test for correlation length $\ell_c = 150\,\text{mm}$.

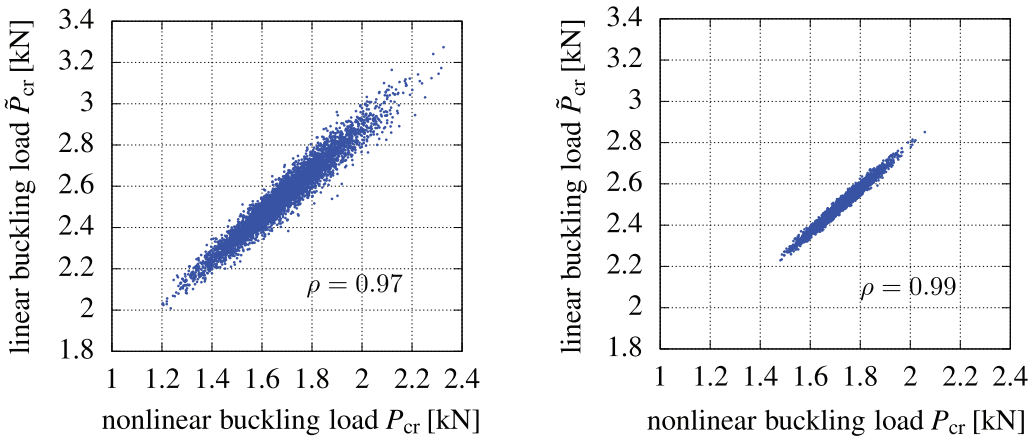

FIGURE 12 | Comparison between buckling loads calculated using non-linear (P_{cr}) and linear analysis ($\tilde{P}_{cr}$) for the correlation lengths $\ell_c = 150\,mm$ (left) and $\ell_c = 500\,mm$ (right).

TABLE 6 | Estimates of second-order statistics for the buckling load of the composite shell panel.

Approach	Monte Carlo	Control Variates with splitting	Monte Carlo	Control Variates with splitting
ℓ_c [mm]		150		500
n	600	90	600	60
m	—	999	—	900
n_e	600	285	600	227
$\widehat{\mu_1'}$ kN	1.7	1.69	1.72	1.73
$V\left[\widehat{\mu_1'}\right]$ kN^2	5×10^{-5}	4.1×10^{-5}	1.0×10^{-5}	8.1×10^{-6}
$\delta_{\widehat{\mu_1'}}$	0.4%	0.4%	0.2%	0.2%
$\widehat{\mu_2}$ kN^2	0.03	0.03	0.006	0.006
$V\left[\widehat{\mu_2}\right]$ kN^4	2.8×10^{-6}	2.8×10^{-6}	1.2×10^{-7}	1.0×10^{-7}
$\delta_{\widehat{\mu_2}}$	5.6%	5.8%	5.6%	5.6%
$\delta_{P_{cr}}$	10.2%	10%	4.6%	4.4%

linear solutions is 4.8 times faster than performing the non-linear buckling analyses. However, for the small correlation length, the subspace eigenvalue solver sometimes requires more iteration steps to compute the correct eigenvalue. This means that the chosen eigenvalue solver and its properties significantly influence the effectiveness of the Control Variates approach.

The results of the estimates of second-order statistics using the Control Variates approach are provided for both correlation lengths in Table 6. The estimates produced using Monte Carlo and Control Variates with Splitting are practically identical in terms of both accuracy and precision, measured in terms of the coefficient of variation δ in Table 6.

For a smaller correlation length $\ell_c = 150\,\text{mm}$, the time factor between linear and non-linear buckling analysis is $f_s = 5.58$. According to Equation (33), it follows an equivalent number of $n_e = 285$ simulations using the Control Variates approach. Compared to an equivalent number of $n_e = 600$ Monte Carlo simulations, the proposed approach is approximately $600/285 \approx 2.1$ times faster. For the larger correlation length, the factor between linear and non-linear buckling analysis increases to $f_s = 5.75$, as the subspace eigenvalue solver converges faster for smoother imperfection shapes. In addition, the equivalent number decreases to $n_e = 227$ compared to $n_e = 285$ for the smaller correlation length. This can be explained by analyzing Figure 12, as the correlation coefficient between linear and non-linear buckling loads is $\rho = 0.99$, which is larger than the correlation coefficient associated with a shorter correlation length. In other words, for the case of a longer correlation length, linear buckling analysis provides a better approximation for calculating the exact buckling load. This results in better performance of the Control Variates method, with a speed-up factor of approximately $600/227 \approx 2.6$.

As a final remark, when examining the results of Table 6, it is observed that while the mean buckling load increases slightly with the correlation length, the variance decreases considerably. This is a very interesting behavior, as in problems of linear static stochastic FE analysis, usually the opposite behavior is observed [40, 41]. This highlights the non-linear nature of the problem at hand.

5.3 | Composite Cylinder

Buckling analysis of cylindrical shells is particularly challenging from both theoretical and numerical perspectives, and it is associated with high computational costs. Therefore, the effectiveness of the Control Variates method is investigated for an imperfection-sensitive composite cylinder subjected to random geometric imperfections. For this purpose, cylinder Z23, derived from References [42, 43], is analyzed. The corresponding FE model is depicted in Figure 13.

The cylinder has a length of $L = 510\,\text{mm}$ and a radius of $R = 250\,\text{mm}$, resulting in a circumference approximately three times larger than its length. Based on a convergence study, an FE mesh with 240 shell elements in the circumferential direction and 80 elements in the axial direction is chosen. This approximately regular FE mesh effectively captures the critical buckling modes and is used as the high-fidelity model for the non-linear buckling analysis. In contrast, a coarser mesh of 120×40 elements is used as a low-fidelity model to perform the linear buckling analysis within the Control Variates approach. The cylinder's laminate consists of 10 layers with a stacking sequence of $[\pm 60^\circ, 0^\circ_2, \pm 68^\circ, \pm 52^\circ, \pm 37^\circ]$, corresponding to the fiber orientation φ depicted in Figure 13. A single layer has a thickness of 0.125 mm, leading to a total shell thickness of $t = 1.25\,\text{mm}$. The material parameters are given in Table 7.

The cylinder is clamped at both ends. At the lower edge, the boundary conditions are $u = v = w = 0, \varphi_x = \varphi_y = 0$. Only vertical displacements of the nodes at the upper edge are allowed, $u = u_a$, while $v = w = 0, \varphi_x = \varphi_y = 0$ remain fixed. The resulting axial load is computed as $P = 2\pi Rp$ for an increasing vertical displacement u_a using the arc-length method. The displacement step size significantly influences the computational time. Therefore, five initial coarse displacement steps of $\Delta u_a = 0.1\,\text{mm}$ are applied. These coarse steps are estimated based on the lowest expected buckling load of the cylinder under random imperfections. Subsequently, the cylinder is further loaded with a smaller displacement step size of $\Delta u_a = 0.01\,\text{mm}$ until the first zero diagonal element D_{ii} occurs in the tangent stiffness matrix.

In this example, the random geometric imperfections are generated using the EOLE (Expansion Optimal Linear Estimation) method from Reference [44]. The method allows representing the random field with only a few random variables by minimizing the variance error. The main advantage is that the covariance matrix is required only on a subset of field nodes, the so-called "random field mesh." Thus, a coarser mesh can be defined for the random

TABLE 7 | Material parameters for the composite cylinder Z23.

E_{11} [N/mm²]	E_{22} [N/mm²]	G_{12} [N/mm²]	G_{23} [N/mm²]	ν_{12} [−]
123,550	8,708	5,695	3,400	0.319

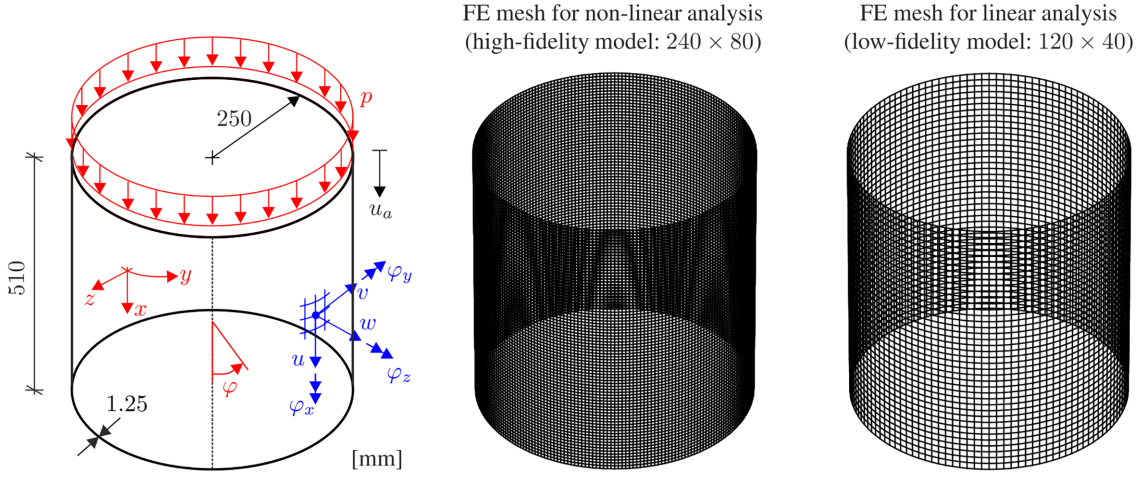

FIGURE 13 | FE model of the composite cylinder.

field compared to the finer mesh required for the FE analysis. The expression for the series to compute random radial imperfections of the cylinder is

$$\hat{w}_{\text{rad}}(\boldsymbol{x},\theta) = \mu + \left(\sum_{i=1}^{M} \frac{\xi_i(\theta)}{\sqrt{\lambda_i}} \, \varphi_i(\boldsymbol{x}^S) \right) C(\boldsymbol{x}^S, \boldsymbol{x}) \tag{38}$$

with the standard normal distributed random variable $\xi_i(\theta)$, the vector $\boldsymbol{x}^S = [\boldsymbol{x}_1 \ \ldots \ \boldsymbol{x}_i^S \ \ldots \ \boldsymbol{x}_M^S]$ of M random field nodes and the vector $\boldsymbol{x} = [\boldsymbol{x}_1 \ \ldots \ \boldsymbol{x}_j \ \ldots \ \boldsymbol{x}_N]$ of N nodes in the full domain (e.g., FE nodes). Consequently, $C(\boldsymbol{x}^S, \boldsymbol{x})$ denotes the covariance matrix, which contains the covariances between random field nodes and FE nodes. The eigenfunctions $\varphi_i(\boldsymbol{x}^S)$ and eigenvalues λ_i are obtained from the covariance matrix $C(\boldsymbol{x}_i^S, \boldsymbol{x}_j^S)$ based on the random field mesh. Both covariance matrices $C(\boldsymbol{x}^S, \boldsymbol{x})$ and $C(\boldsymbol{x}^S, \boldsymbol{x}^S)$ are calculated using the homogeneous correlation structure in Equation (36) and the Whittle–Matérn autocorrelation function in Equation (37). Depending on the smoothness of the random field, the number of random field nodes can be smaller than the number of FE nodes. This allows reducing the size of the eigenvalue problem of the covariance matrix. In this example, a random field mesh with $M = 60 \times 20$ nodes is defined based on a convergence study, where the second-order statistics of the buckling load are evaluated. In Equation (38), the constant mean value μ is set to zero and the standard deviation of the field is chosen as $\sigma = 1$. Considering the presented measured geometric imperfections of the cylinder in Reference [43], the random imperfections are scaled to a peak-to-peak value of 2 mm.

In a first study, the stochastic buckling behavior is analyzed for different correlation lengths. The results of the mean $\mu_{P_{\text{cr}}}$ and the coefficient of variation $\delta_{P_{\text{cr}}}$ of the buckling load as functions of the correlation length are depicted in Figure 14.

For each correlation length, a Monte Carlo simulation with 500 samples is performed. In Figure 14 (left), the resulting non-linear buckling load of $P_{\text{cr}} = 261.64\,\text{kN}$ of the cylinder without imperfections is depicted as a horizontal line. Due to the applied scaling of the random geometric imperfections, the mean of the buckling load asymptotically approaches a value below the non-linear buckling load as the correlation length increases. In contrast, the coefficient of variation decreases with increasing correlation length, see Figure 14 (right). A maximum coefficient of variation of $\delta_{P_{\text{cr}}} = \sigma_{P_{\text{cr}}}/\mu_{P_{\text{cr}}} = 7.3\%$ results for the correlation length of $\ell_c = 150\,\text{mm}$, which is selected for the following investigations. With respect to the mean of the buckling load $\mu_{P_{\text{cr}}} = 174.70$ for the chosen correlation length of $\ell_c = 150\,\text{mm}$, the knockdown factor (KDF) is $\mu_{P_{\text{cr}}}/P_{\text{cr}} = 174.7/261.64 = 0.67$.

The load–displacement curves of the composite cylinder with and without random radial imperfections are depicted in Figure 15.

A typical linear pre-buckling behavior of a cylindrical shell can be observed. At the stability point (A) of the cylinder without imperfections, the initial post-buckling mode $\boldsymbol{\varphi}_{\text{cr}}$ is depicted. Due to the clamped edges, where the radial expansion of the cylinder is suppressed, the buckling mode is characterized by radial displacements at the top and bottom of the cylinder. Furthermore, a sample of the scaled radial imperfection is depicted in Figure 14, which corresponds to the blue load–displacement curve and a buckling load of $P_{\text{cr}} = 165.86\,\text{kN}$ (KDF of 0.63).

The buckling load of the linear analysis using the high-fidelity model (FE mesh with 240×80 elements) is $\tilde{P}_{\text{cr}} = 276.96\,\text{kN}$. Whereas, the linear buckling load using the low-fidelity model (FE mesh with 140×40 elements) is $\tilde{P}_{\text{cr}} = 301.02\,\text{kN}$. The model behaves significantly stiffer. However, the correlation between the linear and non-linear analyses decreases only slightly. This can be observed in the correlation plots in Figure 16, where only the model of the linear analysis is changed. The non-linear buckling analysis is performed with the high-fidelity model.

On the given computational setup, the linear analysis using the low-fidelity model is 13 times faster compared to the high-fidelity model. Thus, the effectiveness of the Control Variates method can be enhanced by performing the linear buckling analysis using the low-fidelity model. The results of the Control Variates approach compared to the Monte Carlo simulation are given in Table 8.

According to Equation (33), the Control Variates require only a number of $n_e = 285$ equivalent simulations instead of 390 Monte Carlo simulations. The linear buckling analysis using the low-fidelity model is 20.68 times faster than the non-linear analysis using the high-fidelity model. Considering the equivalent numbers of the Monte Carlo simulation and the Control Variates

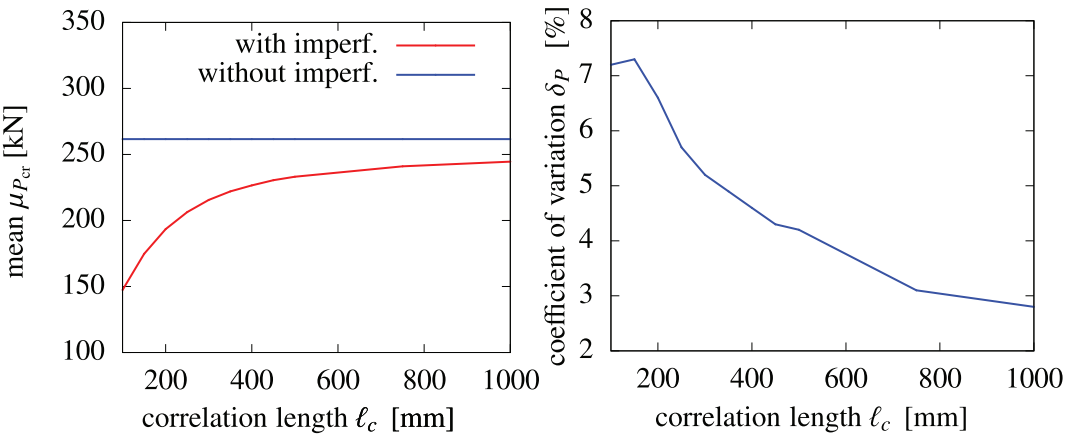

FIGURE 14 | Mean $\mu_{P_{\text{cr}}}$ (left) and coefficient of variation $\delta_{P_{\text{cr}}}$ (right) of the buckling load as a function of the correlation length.

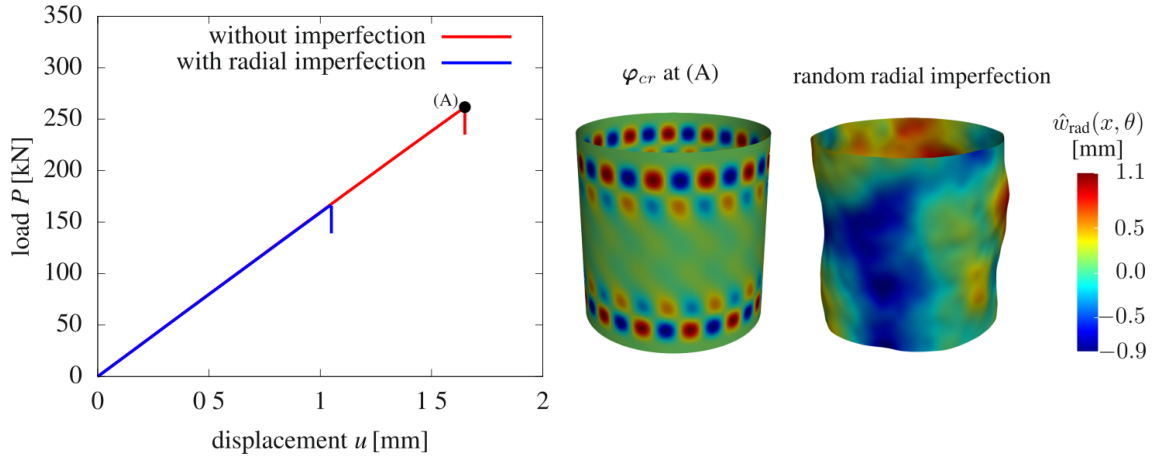

FIGURE 15 | Load–displacement curve of the composite cylinder Z23 with the first eigenvector at the stability point of the cylinder without imperfection and a random radial imperfection, magnified (x20).

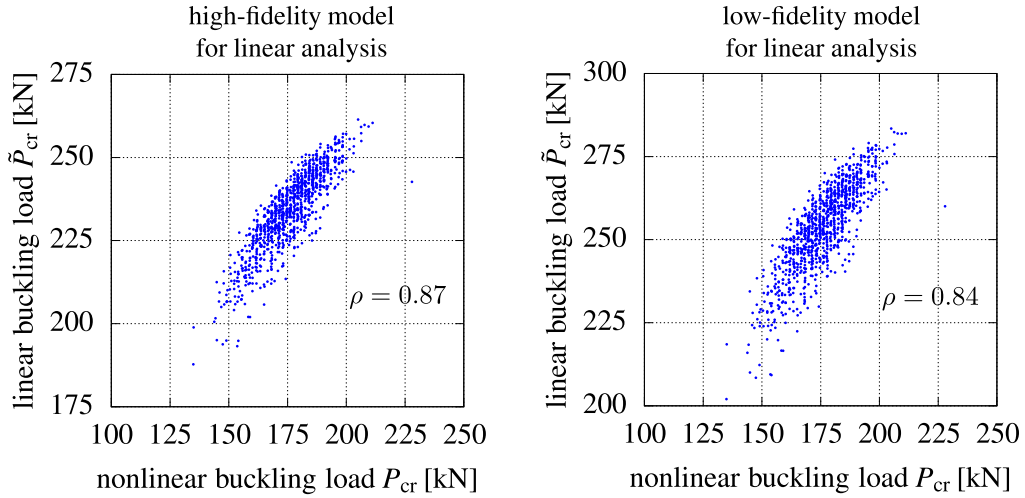

FIGURE 16 | Comparison between buckling loads calculated using non-linear (P_{cr}) and linear analysis ($\tilde{P}_{cr}$) using the high-fidelity model (left) and the low fidelity model (right) for the linear buckling analysis.

TABLE 8 | Estimates of second-order statistics for the buckling load for the composite cylinder.

Approach	Monte Carlo	Control Variates with splitting
n	390	210
m	—	990
n_e	390	268
$\widehat{\mu_1'}$ N	176.5	176.1
$V\left[\widehat{\mu_1'}\right]$ N^2	0.41	0.33
$\delta_{\widehat{\mu_1'}}$	0.4%	0.3%
$\widehat{\mu_2}$ N^2	161.4	154.2
$V\left[\widehat{\mu_2}\right]$ N^4	137.8	129.8
$\delta_{\widehat{\mu_2}}$	7.3%	7.4%
$\delta_{P_{cr}}$	7.2%	7.1%

method, a speed-up factor of approximately $390/268 \approx 1.5$ is achieved. Although the correlation is approximately 10% lower than in the other examples, the computational time is reduced. Thus, the CV method can serve as an effective tool for increasing the efficiency of stochastic analyses in shell buckling.

6 | Conclusions

The paper highlights a promising approach to estimate the second-order statistics of buckling loads. By integrating results from both linear and non-linear buckling analyses, this method achieves enhanced accuracy and significantly reduced computational costs compared to full-scale Monte Carlo simulations. However, the effectiveness of the Control Variates method for buckling problems depends on various factors and can be further optimized. One factor is the eigenvalue solver used for the linear buckling analysis. Therefore, other solvers have to be tested in this context.

Another important factor is the correlation properties of the random geometric imperfections. In this paper, the influence of different correlation lengths is studied, but the correlation function and its differentiability may also influence the computational efficiency of calculating second-order statistics with Control Variates. Defining relevant correlation lengths and functions based on experimental data is essential for quantifying the benefits of Control Variates in realistic scenarios. To account for epistemic uncertainties, correlation parameters can be quantified using polymorphic uncertainty models. The application of the Control Variates method in the context of polymorphic uncertainties (imprecise probabilities) is also conceivable.

Finally, the Control Variates approach should be tested for advanced structures, including stiffened panels and cylindrical shells, fiber-steered composites, and large-scale structures, to assess its broader applicability. New ideas for further research can be summarized as follows:

- Efficient eigenvalue solvers for Control Variates
- Study on the influence of the correlation functions and their differentiability on estimating second-order statistics using Control Variates.
- Application of Control Variates for various structures, such as cylindrical shells, stiffened panels, fiber-steered composites, and large-scale structures
- Application of Control Variates in the framework of polymorphic uncertainties (imprecise probabilities)
- Extension of the current framework from a single variable for performing Control Variates (in this case, buckling load from linear analysis) to several variables (e.g., higher-order buckling loads from linear analysis). It is to be noted that extension towards several variables within the framework of Control Variates is possible, as discussed in, for example, [19].

Acknowledgments

Financial support was provided by the Deutsche Forschungsgemeinschaft (DFG, German Research Foundation) in the framework of project 511267658. This support is gratefully acknowledged. Open Access funding enabled and organized by Projekt DEAL.

Conflicts of Interest

The authors declare no conflicts of interest.

Data Availability Statement

The data and materials that support the findings of this paper are available upon request to the corresponding author.

References

1. H. Wagner, C. Hühne, and I. Elishakoff, "Probabilistic and Deterministic Lower-Bound Design Benchmarks for Cylindrical Shells Under Axial Compression," *Thin-Walled Structures* 146 (2020): 106451.

2. M. Broggi and G. Schuëller, "Efficient Modeling of Imperfections for Buckling Analysis of Composite Cylindrical Shells," *Engineering Structures* 33, no. 5 (2011): 1796–1806.

3. S. Lauterbach, M. Fina, and W. Wagner, "Influence of Stochastic Geometric Imperfections on the Load-Carrying Behaviour of Thin-Walled Structures Using Constrained Random Fields," *Computational Mechanics* 62, no. 5 (2018): 1107–1125.

4. C. Schenk and G. Schuëller, "Buckling Analysis of Cylindrical Shells With Random Geometric Imperfections," *International Journal of Non-Linear Mechanics* 38, no. 7 (2003): 1119–1132.

5. M. Fina, *Polymorphe Unschärfemodellierung in der nichtlinearen Strukturmechanik – Stabilität von Schalentragwerken, räumliche Variabilität und Metamodellierung, Phd-thesis* (Institut für Baustatik, Karlsruher Institut für Technologie, 2020), https://doi.org/10.5445/IR/1000129960.

6. M. Fina, P. Weber, and W. Wagner, "Polymorphic Uncertainty Modeling for the Simulation of Geometric Imperfections in Probabilistic Design of Cylindrical Shells," *Structural Safety* 82 (2020): 101894.

7. M. Fina, L. Panther, P. Weber, and W. Wagner, "Shell Buckling With Polymorphic Uncertain Surface Imperfections and Sensitivity Analysis," *ASCE-ASME Journal of Risk and Uncertainty in Engineering Systems Part B: Mechanical Engineering* 7, no. 2 (2021): 020909.

8. W. Graf, M. Götz, and M. Kaliske, "Analysis of Dynamical Processes Under Consideration of Polymorphic Uncertainty," *Structural Safety* 52 (2015): 194–201.

9. M. Beer, S. Ferson, and V. Kreinovich, "Imprecise Probabilities in Engineering Analyses," *Mechanical Systems and Signal Processing* 37, no. 1 (2013): 4–29.

10. M. Faes and D. Moens, "Recent Trends in the Modeling and Quantification of Non-Probabilistic Uncertainty," *Archives of Computational Methods in Engineering* 27, no. 3 (2019): 633–671.

11. M. Fina, W. Wagner, and W. Graf, "On Polymorphic Uncertainty Modeling in Shell Buckling," *Computer-Aided Civil and Infrastructure Engineering* 38, no. 18 (2023): 2632–2647.

12. M. Fina and C. Bisagni, "Buckling Design Optimization of Tow-Steered Composite Panels and Cylindrical Shells Considering Aleatory and Epistemic Uncertainties," *Computational Mechanics* (2025), https://doi.org/10.1007/s00466-024-02589-8.

13. E. Barbero, A. Madeo, G. Zagari, R. Zinno, and G. Zucco, "Imperfection Sensitivity Analysis of Laminated Folded Plates," *Thin-Walled Structures* 90 (2015): 128–139.

14. G. Garcea, F. S. Liguori, L. Leonetti, D. Magisano, and A. Madeo, "Accurate and Efficient a Posteriori Account of Geometrical Imperfections in Koiter Finite Element Analysis," *International Journal for Numerical Methods in Engineering* 112, no. 9 (2017): 1154–1174.

15. P. Hao, Y. Duan, D. Liu, H. Yang, D. Liu, and B. Wang, "Image-Driven Intelligent Prediction of Buckling Behavior for Geometrically Imperfect Cylindrical Shells," *AIAA Journal* 61, no. 5 (2023): 2266–2280.

16. M. Schweizer, M. Fina, W. Wagner, and S. Freitag, "Artificial Neural Networks for Random Fields to Predict the Buckling Load of Geometrically Imperfect Structures," *Computational Mechanics* (2025), https://doi.org/10.1007/s00466-024-02595-w.

17. S. Freitag, P. Edler, K. Kremer, and G. Meschke, "Multilevel Surrogate Modeling Approach for Optimization Problems With Polymorphic Uncertain Parameters," *International Journal of Approximate Reasoning* 119 (2020): 81–91.

18. M. Fina, C. Lauff, M. Faes, M. Valdebenito, W. Wagner, and S. Freitag, "Bounding Imprecise Failure Probabilities in Structural Mechanics Based on Maximum Standard Deviation," *Structural Safety* 101 (2023): 102293.

19. A. Avramidis and J. Wilson, "A Splitting Scheme for Control Variates," *Operations Research Letters* 14, no. 4 (1993): 187–198.

20. C. Acevedo, M. Valdebenito, I. González, H. Jensen, M. Faes, and Y. Liu, "Control Variates With Splitting for Aggregating Results of Monte Carlo Simulation and Perturbation Analysis," *Structural Safety* 108 (2024): 102445.

21. T. S. Charlton, M. Rouainia, and R. J. Dawson, "Control Variate Approach for Efficient Stochastic Finite-Element Analysis of Geotechnical Problems," *ASCE-ASME Journal of Risk and Uncertainty in Engineering Systems, Part A: Civil Engineering* 4, no. 3 (2018): 04018031.

22. M. Rashki, A. Ghavidel, H. G. Arab, and S. Mousavi, "Low-Cost Finite Element Method-Based Reliability Analysis Using Adjusted Control Variate Technique," *Structural Safety* 75 (2018): 133–142.

23. W. Wagner, "A Note on FEM Buckling Analysis," *Communications in Numerical Methods in Engineering* 11, no. 2 (1995): 149–158.

24. W. Wagner and P. Wriggers, "A Simple Method for the Calculation of Postcritical Branches," *Engineering Computations* 5, no. 2 (1988): 103–109.

25. A. Spence and A. D. Jepson, *The Numerical Calculation of Cusps, Bifurcation Points and Isola Formation Points in Two Parameter Problems* (Birkhäuser Basel, 1984), 502–514, https://doi.org/10.1007/978-3-0348-6256-1_35.

26. P. Wriggers, W. Wagner, and C. Miehe, "A Quadratically Convergent Procedure for the Calculation of Stability Points in Finite Element Analysis," *Computer Methods in Applied Mechanics and Engineering* 70, no. 3 (1988): 329–347.

27. O. Ditlevsen and H. Madsen, *Structural Reliability Methods* (John Wiley and Sons, 1996).

28. G. Fishman, *Monte Carlo: Concepts, Algorithms and Applications* (Springer, 1996).

29. A. Ang and W. Tang, *Probability Concepts in Engineering: Emphasis on Applications to Civil and Environmental Engineering* (Wiley, 2007).

30. B. Nelson, "Control Variate Remedies," *Operations Research* 38, no. 6 (1990): 974–992.

31. W. Wagner and F. Gruttmann, "A Robust Non-Linear Mixed Hybrid Quadrilateral Shell Element," *International Journal for Numerical Methods in Engineering* 64, no. 5 (2005): 635–666.

32. R. L. Taylor, "Finite Element Analysis Program (FEAP)," (2025), http://www.ce.berkeley.edu/projects/feap/.

33. K.-J. Bathe, *Finite Element Procedures*, 1st ed. (Prentice Hall, Pearson Education, Inc., 2006).

34. T. J. R. Hughes, *The Finite Element Method: Linear Static and Dynamic Finite Element Analysis* (Dover Publications, 2000).

35. W. Wagner and F. Gruttmann, "A Simple Finite Rotation Formulation for Composite Shell Elements," *Engineering Computations* 11, no. 2 (1994): 145–176.

36. B. Sudret and A. D. Kiureghian, "Stochastic Finite Element Methods and Reliability–A State-of-the-Art Report," 2000.

37. E. Vanmarcke, *Random Fields: Analysis and Synthesis* (World Scientific, 2010).

38. J. Ching and K.-K. Phoon, "Impact of Autocorrelation Function Model on the Probability of Failure," *Journal of Engineering Mechanics* 145, no. 1 (2019): 04018123.

39. M. Faes, M. Broggi, P. Spanos, and M. Beer, "Elucidating Appealing Features of Differentiable Auto-Correlation Functions: A Study on the Modified Exponential Kernel," *Probabilistic Engineering Mechanics* 69 (2022): 103269.

40. G. Deodatis, "Bounds on Response Variability of Stochastic Finite Element Systems: Effect of Statistical Dependence," *Probabilistic Engineering Mechanics* 5, no. 2 (1990): 88–98.

41. F. Yamazaki, M. Shinozuka, and G. Dasgupta, "Neumann Expansion for Stochastic Finite Element Analysis," *Journal of Engineering Mechanics* 114, no. 8 (1988): 1335–1354.

42. H.-R. Meyer-Piening, M. Farshad, B. Geier, and R. Zimmermann, "Buckling Loads of Cfrp Composite Cylinders Under Combined Axial and Torsion Loading–Experiments and Computations," *Composite Structures* 53, no. 4 (2001): 427–435.

43. H. Wagner, C. Hühne, and M. Janssen, "Buckling of Cylindrical Shells Under Axial Compression With Loading Imperfections: An Experimental and Numerical Campaign on Low Knockdown Factors," *Thin-Walled Structures* 151 (2020): 106764.

44. C. Li and A. Kiureghian, "Optimal Discretization of Random Fields," *Journal of Engineering Mechanics* 119, no. 6 (1993): 1136–1154.

45. B. Stokes, "MathStatica 2.5," *Journal of Statistical Software, Software Reviews* 47, no. 1 (2012): 1–12.

Appendix A

Bivariate Central Co-Moments

Bivariate central co-moments between the non-linear buckling load P_{cr} and linear buckling load $\tilde{P}_{\mathrm{cr}}$ are denoted as $\mu_{p,q}(P_{\mathrm{cr}}, \tilde{P}_{\mathrm{cr}})$, where the pair of integer numbers p and q represent the order associated with P_{cr} and $\tilde{P}_{\mathrm{cr}}$, respectively. Monte Carlo simulation is employed to estimate these co-moments considering a sample set $\boldsymbol{\Xi}_l$ with l independent, identically distributed samples of $\boldsymbol{\Xi}$. The list of co-moments required to implement the expressions in this paper is listed below. This list has been produced using the software package *mathStatica* [45]. Note that the expressions below consider the auxiliary variable $s_{p,q}$, which is defined as $s_{p,q} = \sum_{i=1}^{l} \left(P_{\mathrm{cr}}\left(\boldsymbol{\xi}^{(i)}\right)\right)^p \left(\tilde{P}_{\mathrm{cr}}\left(\boldsymbol{\xi}^{(i)}\right)\right)^q$, where $\boldsymbol{\xi}^{(i)}$ is the i-th sample of the sample set $\boldsymbol{\Xi}_l$.

$$\widehat{\mu_{1,1}} = \frac{l s_{1,1} - s_{0,1} s_{1,0}}{(l-1)l} \tag{A1}$$

$$\begin{aligned}\widehat{\mu_{2,2}} = \frac{1}{(l-3)(l-2)(l-1)l}\Big(&\left(-2l^2+4l-6\right)s_{2,1}s_{0,1} + \left(-2l^2+4l-6\right)s_{1,0}s_{1,2} \\ &+ \left(l^3-2l^2+3l\right)s_{2,2} + l s_{2,0}s_{0,1}^2 + 4l s_{1,0}s_{1,1}s_{0,1} + l s_{0,2}s_{1,0}^2 \\ &+ (6-4l)s_{1,1}^2 + (3-2l)s_{0,2}s_{2,0} - 3s_{1,0}^2 s_{0,1}^2\Big)\end{aligned} \tag{A2}$$

$$\begin{aligned}\widehat{\mu_{4,0}} = \frac{1}{(l-3)(l-2)(l-1)l}\Big(&\left(-4l^2+8l-12\right)s_{3,0}s_{1,0} \\ &+\left(l^3-2l^2+3l\right)s_{4,0} + 6l s_{2,0}s_{1,0}^2 + (9-6l)s_{2,0}^2 - 3s_{1,0}^4\Big)\end{aligned} \tag{A3}$$

$$\begin{aligned}\widehat{\mu_{0,4}} = \frac{1}{(l-3)(l-2)(l-1)l}\Big(&\left(-4l^2+8l-12\right)s_{0,3}s_{0,1} \\ &+\left(l^3-2l^2+3l\right)s_{0,4} + 6l s_{0,2}s_{0,1}^2 + (9-6l)s_{0,2}^2 - 3s_{0,1}^4\Big)\end{aligned} \tag{A4}$$

Squared co-moments as well as co-moment products are estimated with the equations listed below [45].

$$\begin{aligned}\widehat{\mu_{1,1}^2} = \frac{1}{(l-3)(l-2)(l-1)l}\Big(&\left(l^2-3l+2\right)s_{1,1}^2 + \left(l-l^2\right)s_{2,2} \\ &+ (2-2l)s_{1,0}s_{1,1}s_{0,1} + (2l-2)s_{2,1}s_{0,1} + (2l-2)s_{1,0}s_{1,2} \\ &+ s_{1,0}^2 s_{0,1}^2 - s_{2,0}s_{0,1}^2 - s_{0,2}s_{1,0}^2 + s_{0,2}s_{2,0}\Big)\end{aligned} \tag{A5}$$

$$\widehat{\mu_{2,0}^2} = \frac{\begin{aligned}&\left(l^2-3l+3\right)s_{2,0}^2 + \left(l-l^2\right)s_{4,0} - 2l s_{2,0}s_{1,0}^2 \\ &+(4l-4)s_{3,0}s_{1,0} + s_{1,0}^4\end{aligned}}{(l-3)(l-2)(l-1)l} \tag{A6}$$

$$\widehat{\mu_{0,2}^2} = \frac{\begin{aligned}&\left(l^2-3l+3\right)s_{0,2}^2 + \left(l-l^2\right)s_{0,4} - 2l s_{0,2}s_{0,1}^2 \\ &+(4l-4)s_{0,3}s_{0,1} + s_{0,1}^4\end{aligned}}{(l-3)(l-2)(l-1)l} \tag{A7}$$

$$\begin{aligned}\widehat{\mu_{2,0}\mu_{0,2}} = \frac{1}{(l-3)(l-2)(l-1)l}\Big(&\left(l^2-3l+1\right)s_{0,2}s_{2,0} \\ &+ \left(l-l^2\right)s_{2,2} + (2-l)s_{2,0}s_{0,1}^2 + (2l-2)s_{2,1}s_{0,1} \\ &+ (2-l)s_{0,2}s_{1,0}^2 + (2l-2)s_{1,0}s_{1,2} \\ &+s_{1,0}^2 s_{0,1}^2 - 4s_{1,0}s_{1,1}s_{0,1} + 2s_{1,1}^2\Big)\end{aligned} \tag{A8}$$